ASTROPHYSICAL GYROKINETICS: BASIC EQUATIONS AND LINEAR THEORY

Gregory G. Howes,[1] Steven C. Cowley,[2,3] William Dorland,[4] Gregory W. Hammett,[5]
Eliot Quataert,[1] and Alexander A. Schekochihin[6]

ABSTRACT

Magnetohydrodynamic (MHD) turbulence is encountered in a wide variety of astrophysical plasmas, including accretion disks, the solar wind, and the interstellar and intracluster medium. On small scales, this turbulence is often expected to consist of highly anisotropic fluctuations with frequencies small compared to the ion cyclotron frequency. For a number of applications, the small scales are also collisionless, so a kinetic treatment of the turbulence is necessary. We show that this anisotropic turbulence is well described by a low-frequency expansion of the kinetic theory called gyrokinetics. This paper is the first in a series to examine turbulent astrophysical plasmas in the gyrokinetic limit. We derive and explain the nonlinear gyrokinetic equations and explore the linear properties of gyrokinetics as a prelude to nonlinear simulations. The linear dispersion relation for gyrokinetics is obtained, and its solutions are compared to those of hot-plasma kinetic theory. These results are used to validate the performance of the gyrokinetic simulation code GS2 in the parameter regimes relevant for astrophysical plasmas. New results on global energy conservation in gyrokinetics are also derived. We briefly outline several of the problems to be addressed by future nonlinear simulations, including particle heating by turbulence in hot accretion flows and in the solar wind, the magnetic and electric field power spectra in the solar wind, and the origin of small-scale density fluctuations in the interstellar medium.

Subject headings: methods: numerical — MHD — turbulence

1. INTRODUCTION

The Goldreich & Sridhar (1995, hereafter GS95) theory of MHD turbulence (see also Sridhar & Goldreich 1994; Goldreich & Sridhar 1997; Lithwick & Goldreich 2001) in a mean magnetic field predicts that the energy cascades primarily by developing small scales perpendicular to the local field, with $k_\perp \gg k_\parallel$, as schematically shown in Figure 1 (cf. earlier work by Montgomery & Turner 1981; Shebalin et al. 1983). Numerical simulations of magnetized turbulence with a dynamically strong mean field support the idea that such a turbulence is strongly anisotropic (Maron & Goldreich 2001; Cho et al. 2002). In situ measurements of turbulence in the solar wind (Belcher & Davis 1971; Matthaeus et al. 1990) and observations of interstellar scintillation (Wilkinson et al. 1994; Trotter et al. 1998; Rickett et al. 2002; Dennett-Thorpe & de Bruyn 2003) also provide evidence for significant anisotropy.

In many astrophysical environments, small-scale perturbations in the MHD cascade have (parallel) wavelengths much smaller than, or at least comparable to, the ion mean free path, implying that the turbulent dynamics should be calculated using kinetic theory. As a result of the intrinsic anisotropy of MHD turbulence, the small-scale perturbations also have frequencies well below the ion cyclotron frequency, $\omega \ll \Omega_i$, even when the perpendicular wavelengths are comparable to the ion gyroradius (see Fig. 1).

Anisotropic MHD turbulence in plasmas with weak collisionality can be described by a system of equations called gyrokinetics.

Particle motion in the small-scale turbulence is dominantly the cyclotron motion about the unperturbed field lines. Gyrokinetics exploits the timescale separation ($\omega \ll \Omega_i$) for the electromagnetic fluctuations to eliminate 1 degree of freedom in the kinetic description, thereby reducing the problem from six to five dimensions (three spatial plus two in velocity space). It does so by averaging over the fast cyclotron motion of charged particles in the mean magnetic field. The resulting "gyrokinetic" equations describe charged "rings" moving in the ring-averaged electromagnetic fields. The removal of one dimension of phase space and the fast cyclotron timescale achieves a more computationally efficient treatment of low-frequency turbulent dynamics. The gyrokinetic system is completed by electromagnetic field equations that are obtained by applying the gyrokinetic approximation to Maxwell's equations. The gyrokinetic approximation orders out the fast MHD wave and the cyclotron resonance but retains finite Larmor-radius effects, collisionless dissipation via the parallel Landau resonance, and collisions. Both the slow MHD wave and the Alfvén wave are captured by the gyrokinetics, although the former is damped when its wavelength along the magnetic field is smaller than the ion mean free path (Barnes 1966; Foote & Kulsrud 1979).

Linear (Rutherford & Frieman 1968; Taylor & Hastie 1968; Catto 1978; Antonsen & Lane 1980; Catto et al. 1981) and nonlinear gyrokinetic theory (Frieman & Chen 1982; Dubin et al. 1983; Lee 1983, 1987; Hahm et al. 1988; Brizard 1992) has proven to be a valuable tool in the study of laboratory plasmas. It has been extensively employed to study the development of turbulence driven by microinstabilities, e.g., the ion and electron temperature-gradient instabilities (e.g., Dimits et al. 1996; Dorland et al. 2000; Jenko et al. 2000, 2001; Rogers et al. 2000; Jenko & Dorland 2001, 2002; Candy et al. 2004; Parker et al. 2004). For these applications, the structure of the mean equilibrium field and the

[1] Department of Astronomy, 601 Campbell Hall, University of California, Berkeley, CA 94720; ghowes@astro.berkeley.edu.
[2] Department of Physics and Astronomy, University of California, Los Angeles, CA 90095-1547.
[3] Department of Physics, Imperial College London, Blackett Laboratory, Prince Consort Road, London SW7 2BW, UK.
[4] Department of Physics, University of Maryland, College Park, MD 20742-3511.
[5] Princeton University Plasma Physics Laboratory, P.O. Box 451, Princeton, NJ 08543.
[6] Department of Applied Mathematics and Theoretical Physics, University of Cambridge, Wilberforce Road, Cambridge CB3 0WA, UK.
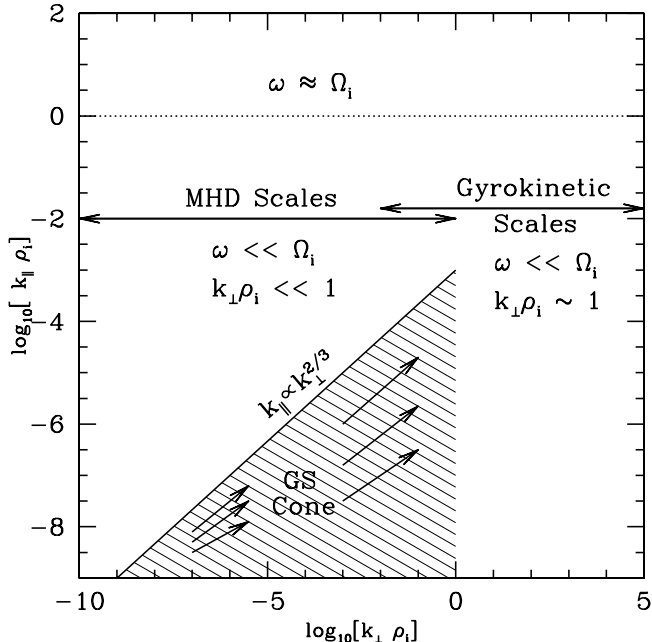
FIG. 1.—Schematic diagram of the low-frequency, anisotropic Alfvén wave cascade in wavenumber space. The horizontal axis is perpendicular wavenumber; the vertical axis is the parallel wavenumber, proportional to the frequency. MHD (or, rather, strictly speaking, its Alfvén wave part; see Schekochihin et al. 2006) is valid only in the limit $\omega \ll \Omega_i$ and $k_\perp \rho_i \ll 1$; gyrokinetic theory remains valid when the perpendicular wavenumber is of the order of the ion Larmor radius, $k_\perp \rho_i \sim 1$. Note that $\omega \to \Omega_i$ only when $k_\parallel \rho_i \to 1$, so gyrokinetics is applicable for $k_\parallel \ll k_\perp$.

TABLE 1
DEFINITIONS OF PLASMA PARAMETERS

Parameter	Definition
s	Particle species
m_s	Particle mass
q_s	Particle charge (we take $q_i = -q_e = e$)
n_{0s}	Number density
T_{0s}	Temperature (in units of energy)
$\beta_s = 8\pi n_{0s} T_{0s}/B_0^2$	Plasma β
$v_{\mathrm{th}_s} = (2T_{0s}/m_s)^{1/2}$	Thermal speed
$c_s = (T_{0e}/m_i)^{1/2}$	Sound speed
$v_A = B_0/(4\pi m_i n_{0i})^{1/2}$	Alfvén speed
c	Speed of light
$\Omega_s = q_s B_0/(m_s c)$	Cyclotron frequency (carries sign of q_s)
$\rho_s = v_{\mathrm{th}_s}/\Omega_s$	Larmor radius

§ 2.5. In § 2.6, we introduce the linear collisionless dispersion relation of the gyrokinetic theory (detailed derivation is given in Appendix C, and various analytical limits are worked out in Appendix D). The numerics are presented in § 3, where we compare the gyrokinetic dispersion relation and its analytically tractable limits with the full dispersion relation of the hot-plasma theory and with numerical results from the gyrokinetic simulation code GS2. We also discuss the effect of collisions on collisionless damping rates (§ 3.5) and illustrate the limits of applicability of the gyrokinetic approximation (§ 3.6). Finally, § 4 summarizes our results and discusses several potential astrophysical applications of gyrokinetics. Definitions adopted for plasma parameters in this paper are given in Table 1.

2. GYROKINETICS

In this section we describe the gyrokinetic approximation and present the gyrokinetic equations themselves in a simple and physically motivated manner (the details of the derivations are given in Appendices A–D). To avoid obscuring the physics with the complexity of gyrokinetics in full generality, we treat the simplified case of a plasma in a straight, uniform mean magnetic field, $\boldsymbol{B}_0 = B_0 \hat{\boldsymbol{z}}$ and with a spatially uniform equilibrium distribution function, $\nabla F_0 = 0$ (the slab limit). This case also has the most direct astrophysical relevance because the mean gradients in turbulent astrophysical plasmas are generally dynamically unimportant on length scales comparable to the ion gyroradius.

2.1. The Gyrokinetic Ordering

The most basic assumptions that must be satisfied for the gyrokinetic equations to be applicable are weak coupling, strong magnetization, low frequencies, and small fluctuations. The weak coupling is the standard assumption of plasma physics: $n_{0e}\lambda_{De}^3 \gg 1$, where n_{0e} is the mean electron number density and λ_{De} is the electron Debye length. This approximation allows the use of the Fokker-Planck equation to describe the kinetic evolution of all plasma species.

The conditions of strong magnetization and low frequencies in gyrokinetics mean that the ion Larmor radius ρ_i must be much smaller than the macroscopic length scale L of the equilibrium plasma and that the frequency of fluctuations ω must be small compared to the ion cyclotron frequency Ω_i,

$$\rho_i = \frac{v_{\mathrm{th}_i}}{\Omega_i} \ll L, \quad \omega \ll \Omega_i. \qquad (1)$$

The latter assumption allows one to average all quantities over the Larmor orbits of particles, one of the key simplifications

---

gradients in mean temperature and density are critical. The full gyrokinetic equations allow for a spatially varying mean magnetic field, temperature, and density. In an astrophysical plasma, the microinstabilities associated with the mean spatial gradients are unlikely to be as important as the MHD turbulence produced by violent large-scale events or instabilities. Our goal is to use gyrokinetics to describe this MHD turbulence on small scales (see Fig. 1). For this purpose, the variation of the large-scale field, temperature, and density is unimportant. We, therefore, consider gyrokinetics in a uniform equilibrium field with no mean temperature or density gradients.

This is the first in a series of papers to apply gyrokinetic theory to the study of turbulent astrophysical plasmas. In this paper, we derive the equations of gyrokinetics in a uniform equilibrium field and explain their physical meaning. We also derive and analyze the linear gyrokinetic dispersion relation in the collisionless regime, including the high-β regime, which is of particular interest in astrophysics. Future papers will present analytical reductions of the gyrokinetic equations in various asymptotic limits (Schekochihin et al. 2006) and nonlinear simulations applied to specific astrophysical problems These simulations use the gyrokinetic simulation code GS2. As part of our continuing tests of GS2, we demonstrate here that it accurately reproduces the frequencies and damping rates of the linear modes.

The remainder of this paper is organized as follows. In § 2, we present the gyrokinetic system of equations, giving a physical interpretation of the various terms and a detailed discussion of the gyrokinetic approximation. A detailed derivation of the gyrokinetic equations in the limit of a uniform, mean magnetic field with no mean temperature or density gradients is presented in Appendix A. Appendix B contains the first published derivation of the long-term transport and heating equations that describe the evolution of the equilibrium plasma—these are summarized in

allowed by the gyrokinetic theory. Note that the assumption of strong magnetization does not require the plasma β (the ratio of the thermal to the magnetic pressure, $\beta = 8\pi p/B^2$) to be small. A high-β plasma can satisfy this constraint as long as the ion Larmor radius is small compared to the gradients of the equilibrium system. In most astrophysical contexts, even a very weak magnetic field meets this requirement.

To derive the gyrokinetic equations, we order the time and length scales in the problem to separate fluctuating and equilibrium quantities. The remainder of this section defines this formal ordering and describes some simple consequences that follow from it.

Two length scales are characteristic of gyrokinetics: the small length scale, which is the ion Larmor radius ρ_i, and the larger length scale l_0, which is here introduced formally and is argued below to be the typical parallel wavelength of the fluctuations. Their ratio defines the fundamental expansion parameter ϵ used in the formal ordering:

$$\epsilon = \frac{\rho_i}{l_0} \ll 1. \quad (2)$$

There are three relevant timescales, or frequencies, of interest. The fast timescale is given by the ion cyclotron frequency Ω_i. The distribution function and the electric and magnetic fields are assumed to be stationary on this timescale. The intermediate timescale corresponds to the frequency of the turbulent fluctuations,

$$\omega \sim \frac{v_{\mathrm{th}_i}}{l_0} \sim O(\epsilon \Omega_i). \quad (3)$$

The slow timescale is connected to the rate of heating in the system, ordered as follows:

$$\frac{1}{t_{\mathrm{heat}}} \sim \epsilon^2 \frac{v_{\mathrm{th}_i}}{l_0} \sim O(\epsilon^3 \Omega_i). \quad (4)$$

The distribution function f of each species s ($=e, i$; the species index is omitted unless necessary) and magnetic and electric fields $\boldsymbol{B}$ and $\boldsymbol{E}$ are split into equilibrium parts (denoted with a subscript 0) that vary at the slow heating rate and fluctuating parts (denoted with δ and a subscript indicating the order in ϵ) that vary at the intermediate frequency ω:

$$f(\boldsymbol{r}, \boldsymbol{v}, t) = F_0(\boldsymbol{v}, t) + \delta f_1(\boldsymbol{r}, \boldsymbol{v}, t) + \delta f_2(\boldsymbol{r}, \boldsymbol{v}, t) + \ldots, \quad (5)$$

$$\boldsymbol{B}(\boldsymbol{r}, t) = \boldsymbol{B}_0 + \delta\boldsymbol{B}(\boldsymbol{r}, t) = B_0\hat{z} + \nabla \times \boldsymbol{A}, \quad (6)$$

$$\boldsymbol{E}(\boldsymbol{r}, t) = \delta\boldsymbol{E}(\boldsymbol{r}, t) = -\nabla\phi - \frac{1}{c}\frac{\partial \boldsymbol{A}}{\partial t}. \quad (7)$$

Let us now list the gyrokinetic ordering assumptions.

Small fluctuations about the equilibrium.—Fluctuating quantities are formally of order ϵ in the gyrokinetic expansion,

$$\frac{\delta f_1}{F_0} \sim \frac{\delta\boldsymbol{B}}{B_0} \sim \frac{\delta\boldsymbol{E}}{(v_{\mathrm{th}_i}/c)B_0} \sim O(\epsilon). \quad (8)$$

Note that although fluctuations are small, the theory is fully non-linear (interactions are strong).

Slow-timescale variation of the equilibrium.—The equilibrium varies on the heating timescale,

$$\frac{1}{F_0}\frac{\partial F_0}{\partial t} \sim O\left(\frac{1}{t_{\mathrm{heat}}}\right) \sim O\left(\epsilon^2 \frac{v_{\mathrm{th}_i}}{l_0}\right). \quad (9)$$

Derivations for laboratory plasmas (Frieman & Chen 1982) have included a large-scale [$\sim O(1/l_0)$] spatial variation of the equilibrium (F_0 and $\boldsymbol{B}_0$)—this we omit. The slow-timescale evolution of the equilibrium, however, is treated for the first time here.

Intermediate-timescale variation of the fluctuating quantities.—The fluctuating quantities vary on the intermediate timescale

$$\omega \sim \frac{1}{\delta f}\frac{\partial \delta f}{\partial t} \sim \frac{1}{|\delta\boldsymbol{B}|}\frac{\partial \delta\boldsymbol{B}}{\partial t} \sim \frac{1}{|\delta\boldsymbol{E}|}\frac{\partial \delta\boldsymbol{E}}{\partial t} \sim O\left(\frac{v_{\mathrm{th}_i}}{l_0}\right). \quad (10)$$

Intermediate-timescale collisions.—The collision rate in gyrokinetics is ordered to be the same as the intermediate timescale

$$\nu \sim O\left(\frac{v_{\mathrm{th}_i}}{l_0}\right) \sim O(\omega). \quad (11)$$

Collisionless dynamics with $\omega > \nu$ are treated correctly as long as $\nu > \epsilon\omega$.

Small-scale spatial variation of fluctuations across the mean field.—Across the mean magnetic field, the fluctuations occur on the small length scale

$$k_\perp \sim \frac{\hat{z} \times \nabla\delta f}{\delta f} \sim \frac{\hat{z} \times \nabla\delta\boldsymbol{B}}{|\delta\boldsymbol{B}|} \sim \frac{\hat{z} \times \nabla\delta\boldsymbol{E}}{|\delta\boldsymbol{E}|} \sim O\left(\frac{1}{\rho_i}\right). \quad (12)$$

Large-scale spatial variation of fluctuations along the mean field.—Along the mean magnetic field the fluctuations occur on the larger length scale

$$k_\parallel \sim \frac{\hat{z} \cdot \nabla\delta f}{\delta f} \sim \frac{\hat{z} \cdot \nabla\delta\boldsymbol{B}}{|\delta\boldsymbol{B}|} \sim \frac{\hat{z} \cdot \nabla\delta\boldsymbol{E}}{|\delta\boldsymbol{E}|} \sim O\left(\frac{1}{l_0}\right). \quad (13)$$

With a small length scale across the field and a large length scale along the field, the typical gyrokinetic fluctuation is highly anisotropic:

$$\frac{k_\parallel}{k_\perp} \sim \frac{\rho_i}{l_0} \sim O(\epsilon). \quad (14)$$

Figure 2 presents a schematic diagram that depicts the length scales associated with the gyrokinetic ordering. The typical perpendicular flow velocity, roughly the $\boldsymbol{E} \times \boldsymbol{B}$ velocity, is

$$\boldsymbol{u}_\perp \sim \frac{c\delta\boldsymbol{E} \times \boldsymbol{B}}{B_0^2} \sim O(\epsilon v_{\mathrm{th}_i}). \quad (15)$$

The typical perpendicular fluid displacement is $\sim u_\perp/\omega \sim 1/k_\perp \sim O(\rho_i)$, as is the field line displacement. Since displacements are of order the perpendicular wavelength or eddy size, the fluctuations are fully nonlinear.

2.2. The Gyrokinetic Ordering and MHD Turbulence

The GS95 theory of incompressible MHD turbulence conjectures that, on sufficiently small scales, fluctuations at all spatial scales always arrange themselves in such a way that the Alfvén timescale and the nonlinear decorrelation timescale are similar, $\omega \sim k_\parallel v_A \sim k_\perp u_\perp$. This is known as the critical balance. A modification of Kolmogorov (1941) dimensional theory based on this additional assumption then leads to the scaling $u_\perp \sim U(k_\perp L)^{-1/3}$, where U and L are the velocity and the scale at which the turbulence is driven, respectively. For a detailed discussion of these results, we refer the reader to Goldreich and Sridhar's original papers or to a review by Schekochihin & Cowley (2006a).
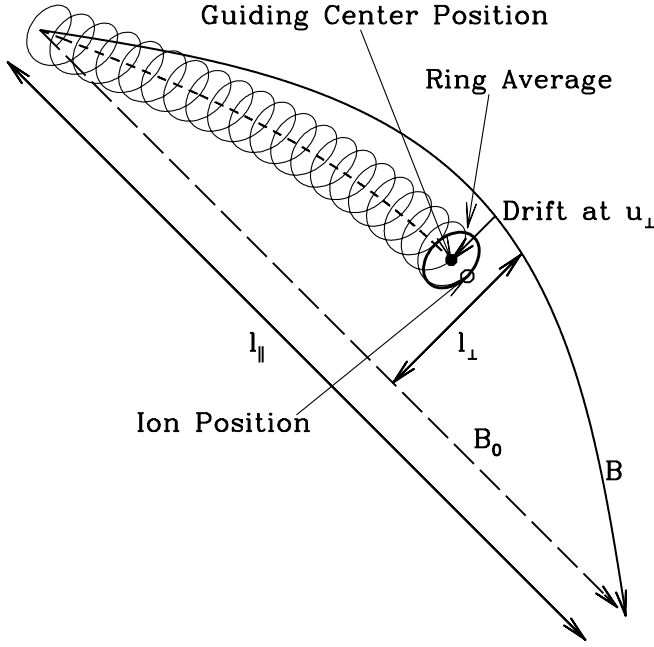
FIG. 2.—Ring average in gyrokinetics. The ion position is given by the open circle, and the guiding center position is given by the filled circle; the ring average, centered on the guiding center position, is denoted by the thick lined circle passing through the particle's position. The characteristic perpendicular and parallel length scales in gyrokinetics are marked $l_\perp$ and $l_\parallel$, respectively; here the perpendicular scale is exaggerated for clarity. The unperturbed magnetic field $\boldsymbol{B}_0$ is given by the long-dashed line, and the perturbed magnetic field $\boldsymbol{B}$ is given by the solid line. The particle drifts off of the field line at $\boldsymbol{u}_\perp$, which is roughly the $\boldsymbol{E} \times \boldsymbol{B}$ velocity.

Here, we show that the gyrokinetic ordering is manifestly consistent with, and indeed can be constructed on the basis of, the GS95 critical balance conjecture. Using the critical balance and the GS95 scaling of $u_\perp$, we find that the ratio of the turbulent frequency $\omega \sim k_\perp u_\perp$ to the ion cyclotron frequency is

$$\frac{\omega}{\Omega_i} \sim \frac{U}{v_{\mathrm{th}_i}} (k_\perp \rho_i)^{2/3} \left(\frac{\rho_i}{L}\right)^{1/3}. \tag{16}$$

The ratio of parallel and perpendicular wavenumbers is

$$\frac{k_\parallel}{k_\perp} \sim \frac{U}{v_A} (k_\perp \rho_i)^{-1/3} \left(\frac{\rho_i}{L}\right)^{1/3}. \tag{17}$$

Both of these ratios have to be order ϵ in the gyrokinetic expansion. Therefore, for the GS95 model of magnetized turbulence, we define the expansion parameter

$$\epsilon = \left(\frac{\rho_i}{L}\right)^{1/3}. \tag{18}$$

Comparing this with equation (2), we may formally define the length scale l_0 used in the gyrokinetic ordering as $l_0 = \rho_i^{2/3} L^{1/3}$. Physically, this definition means that l_0 is the characteristic parallel length scale of the turbulent fluctuations in the context of GS95 turbulence. Note that our assumption of no spatial variation of the equilibrium is, therefore, equivalent to assuming that the variation scale of F_0 and $\boldsymbol{B}_0$ is $\gg l_0$—this is satisfied, e.g., for the injection scale L.

One might worry that the power of $\frac{1}{3}$ in equation (18) means that the expansion is valid only in extreme circumstances. For astrophysical plasmas, however, ρ_i/L is so small that this is prob-

ably not a significant restriction. To take the interstellar medium as a concrete example, $\rho_i \sim 10^8$ cm and $L \sim 100$ pc $\simeq 3 \times 10^{20}$ cm (the supernova scale), so $(\rho_i/L)^{1/3} \sim 10^{-4}$. For galaxy clusters, $(\rho_i/L)^{1/3} \sim 10^{-5}$ (Schekochihin & Cowley 2006b); for hot, radiatively inefficient accretion flows around black holes, $(\rho_i/L)^{1/3} \sim 10^{-3}$ (Quataert 1998); and for the solar wind, $(\rho_i/L)^{1/3} \sim 10^{-2}$.

In the gyrokinetic ordering, all cyclotron-frequency effects (such as the cyclotron resonances) and the fast MHD wave are ordered out (for a more general approach using a kinetic description of plasmas in the gyrocenter coordinates that retains the high-frequency physics, see the gyrocenter gauge theory of Qin et al. [2000]). The slow and Alfvén waves are retained, however, and collisionless dissipation of fluctuations occurs via the Landau resonance, through Landau damping and transit-time, or Barnes (1966), damping. The slow and Alfvén waves are accurately described for arbitrary $k_\perp \rho_i$, as long as they are anisotropic ($k_\parallel \sim \epsilon k_\perp$). Subsidiary ordering of collisions (as long as it does not interfere with the primary gyrokinetic ordering) allows for a treatment of collisionless and/or collisional dynamics. Similarly, subsidiary ordering of the plasma β allows for both low- and high-β plasmas.

The validity of GS95 turbulence theory for compressible astrophysical plasmas is an important question. Direct numerical simulations of compressible MHD turbulence (Cho & Lazarian 2003) demonstrate that spectrum and anisotropy of slow and Alfvén waves are consistent with the GS95 predictions. A recent work exploring weak compressible MHD turbulence in low-β plasmas (Chandran 2006) shows that interactions of Alfvén waves with fast waves produce only a small amount of energy at high $k_\parallel$ (weak turbulence theory for incompressible MHD predicts no energy at high $k_\parallel$), but this is unlikely to alter the prediction of anisotropy in strong turbulence. Both of these works demonstrate that a small amount of fast-wave energy cascades to high frequencies, but the dynamics in this regime are energetically dominated by the low-frequency Alfvén waves.

2.3. Coordinates and Ring Averages

Gyrokinetics is most naturally described in guiding center coordinates, where the position of a particle $\boldsymbol{r}$ and the position of its guiding center $\boldsymbol{R}_s$ are related by

$$\boldsymbol{r} = \boldsymbol{R}_s - \frac{\boldsymbol{v} \times \hat{\boldsymbol{z}}}{\Omega_s}. \tag{19}$$

The particle velocity can be decomposed in terms of the parallel velocity $v_\parallel$, the perpendicular velocity $v_\perp$, and the gyrophase angle θ:

$$\boldsymbol{v} = v_\parallel \hat{\boldsymbol{z}} + v_\perp (\cos\theta \hat{\boldsymbol{x}} + \sin\theta \hat{\boldsymbol{y}}). \tag{20}$$

Gyrokinetics averages over the Larmor motion of particles and describes the evolution of a distribution of rings rather than individual particles. The formalism requires defining two types of ring averages: the ring average at a fixed guiding center $\boldsymbol{R}_s$,

$$\langle a(\boldsymbol{r}, \boldsymbol{v}, t)\rangle_{\boldsymbol{R}_s} = \frac{1}{2\pi} \oint d\theta\, a\left(\boldsymbol{R}_s - \frac{\boldsymbol{v} \times \hat{\boldsymbol{z}}}{\Omega_s}, \boldsymbol{v}, t\right), \tag{21}$$

where the θ integration is done keeping $\boldsymbol{R}_s$, $v_\perp$, and $v_\parallel$ constant, and the ring average at a fixed position $\boldsymbol{r}$,

$$\langle a(\boldsymbol{R}_s, \boldsymbol{v}, t)\rangle_{\boldsymbol{r}} = \frac{1}{2\pi} \oint d\theta\, a\left(\boldsymbol{r} + \frac{\boldsymbol{v} \times \hat{\boldsymbol{z}}}{\Omega_s}, \boldsymbol{v}, t\right), \tag{22}$$

where the integration is at constant $\boldsymbol{r}$, $v_\perp$, and $v_\parallel$.

2.4. *The Gyrokinetic Equations*

The detailed derivation of the gyrokinetic equations is given in Appendix A. Here we summarize the results and their physical interpretation. The full plasma distribution function is expanded as follows:

$$f_s = F_{0s}(v, t) \exp\left[-\frac{q_s \phi(\boldsymbol{r}, t)}{T_{0s}}\right] + h_s(\boldsymbol{R}_s, v, v_\perp, t) + \delta f_{2s} + \dots,$$
(23)

where $v = (v_\perp^2 + v_\parallel^2)^{1/2}$ and the equilibrium distribution function is Maxwellian:

$$F_{0s} = \frac{n_{0s}}{\pi^{3/2} v_{\text{th}_s}^3} \exp\left(-\frac{v^2}{v_{\text{th}_s}^2}\right).$$
(24)

The first-order part of the distribution function is composed of a term that comes from the Boltzmann factor, $\exp\left[-q_s \phi(\boldsymbol{r}, t)/T_{0s}\right] \simeq 1 - q_s \phi(\boldsymbol{r}, t)/T_{0s}$, and the ring distribution h_s. The ring distribution h_s is a function of the guiding center position $\boldsymbol{R}_s$ (not the particle position $\boldsymbol{r}$) and two velocity coordinates, v and $v_\perp$.[7] It satisfies the *gyrokinetic equation*:

$$\frac{\partial h_s}{\partial t} + v_\parallel \hat{\boldsymbol{z}} \cdot \frac{\partial h_s}{\partial \boldsymbol{R}_s} + \frac{c}{B_0}\left[\langle\chi\rangle_{\boldsymbol{R}_s}, h_s\right] - \left(\frac{\partial h_s}{\partial t}\right)_{\text{coll}} = q_s \frac{\partial \langle\chi\rangle_{\boldsymbol{R}_s}}{\partial t} \frac{F_{0s}}{T_{0s}},$$
(25)

where the electromagnetic field enters via the ring average of the gyrokinetic potential $\chi = \phi - \boldsymbol{v} \cdot \boldsymbol{A}/c$. The Poisson bracket is defined by $[U, V] = \hat{\boldsymbol{z}} \cdot [(\partial U/\partial \boldsymbol{R}_s) \times (\partial V/\partial \boldsymbol{R}_s)]$. The scalar potential ϕ and the vector potential $\boldsymbol{A}$ are expressed in terms of h_s via Maxwell's equations: the Poisson's equation, which takes the form of the quasineutrality condition

$$\sum_s q_s \delta n_s = \sum_s \left(-\frac{q_s^2 n_{0s}}{T_{0s}}\phi + q_s \int d^3\boldsymbol{v} \langle h_s\rangle_{\boldsymbol{r}}\right) = 0;$$
(26)

the parallel component of Ampère's law,

$$-\nabla_\perp^2 A_\parallel = \sum_s \frac{4\pi}{c} q_s \int d^3\boldsymbol{v} \, v_\parallel \langle h_s\rangle_{\boldsymbol{r}};$$
(27)

and the perpendicular component of Ampère's law,

$$\nabla_\perp \delta B_\parallel = \sum_s \frac{4\pi}{c} q_s \int d^3\boldsymbol{v} \langle(\hat{\boldsymbol{z}} \times \boldsymbol{v}_\perp) h_s\rangle_{\boldsymbol{r}}.$$
(28)

The gyrokinetic equation (25) can be written in the following, perhaps more physically illuminating, form,

$$\frac{\partial h_s}{\partial t} + \left\langle\frac{d\boldsymbol{R}_s}{dt}\right\rangle_{\boldsymbol{R}_s} \cdot \frac{\partial h_s}{\partial \boldsymbol{R}_s} - \left(\frac{\partial h_s}{\partial t}\right)_{\text{coll}} = \left\langle\frac{d\mathcal{E}_s}{dt}\right\rangle_{\boldsymbol{R}_s} \frac{F_{0s}}{T_{0s}},$$
(29)

where

$$\begin{aligned}
\left\langle\frac{d\boldsymbol{R}_s}{dt}\right\rangle_{\boldsymbol{R}_s} &= v_\parallel \hat{\boldsymbol{z}} - \frac{c}{B_0}\frac{\partial \langle\chi\rangle_{\boldsymbol{R}_s}}{\partial \boldsymbol{R}_s} \times \hat{\boldsymbol{z}} \\
&= v_\parallel \hat{\boldsymbol{z}} - \frac{c}{B_0}\frac{\partial \langle\phi\rangle_{\boldsymbol{R}_s}}{\partial \boldsymbol{R}_s} \times \hat{\boldsymbol{z}} \\
&\quad + \frac{\partial \langle v_\parallel A_\parallel\rangle_{\boldsymbol{R}_s}}{\partial \boldsymbol{R}_s} \times \frac{\hat{\boldsymbol{z}}}{B_0} + \frac{\partial \langle\boldsymbol{v}_\perp \cdot \boldsymbol{A}_\perp\rangle_{\boldsymbol{R}_s}}{\partial \boldsymbol{R}_s} \times \frac{\hat{\boldsymbol{z}}}{B_0}
\end{aligned}$$
(30)

is the ring velocity, $\mathcal{E}_s = (1/2)m_s v^2 + q_s \phi$ is the total energy of the particle, and

$$\left\langle\frac{d\mathcal{E}_s}{dt}\right\rangle_{\boldsymbol{R}_s} = q_s \frac{\partial \langle\chi\rangle_{\boldsymbol{R}_s}}{\partial t}.$$
(31)

Note that the right-hand side of equation (29) is

$$\left\langle\frac{d\mathcal{E}_s}{dt}\right\rangle_{\boldsymbol{R}_s} \frac{F_{0s}}{T_{0s}} = -\left\langle\frac{d\mathcal{E}_s}{dt}\frac{\partial f_s}{\partial \mathcal{E}_s}\right\rangle_{\boldsymbol{R}_s}$$
(32)

written to lowest order in ϵ. Using this and the conservation of the first adiabatic invariant, $\langle d\mu_s/dt\rangle_{\boldsymbol{R}_s} = 0$, where $\mu_s = m_s v_\perp^2/2B_0$, it becomes clear that equation (29) is simply the gyroaveraged Fokker-Planck equation

$$\left\langle\frac{df_s}{dt} - \left(\frac{\partial f_s}{\partial t}\right)_{\text{coll}}\right\rangle_{\boldsymbol{R}_s} = 0,$$
(33)

where only the lowest order in ϵ has been retained.

A simple physical interpretation can now be given for each term in equation (29). It describes the evolution of a distribution of rings h_s that is subject to a number of physical influences:

1. motion of the ring along the ring-averaged total (perturbed) magnetic field: since $\nabla A_\parallel \times \hat{\boldsymbol{z}} = \delta\boldsymbol{B}_\perp$,

$$\left(v_\parallel \hat{\boldsymbol{z}} + \frac{\partial \langle v_\parallel A_\parallel\rangle_{\boldsymbol{R}_s}}{\partial \boldsymbol{R}_s} \times \frac{\hat{\boldsymbol{z}}}{B_0}\right) \cdot \frac{\partial h_s}{\partial \boldsymbol{R}_s} = \left\langle v_\parallel \frac{\boldsymbol{B}}{B_0}\right\rangle_{\boldsymbol{R}_s} \cdot \frac{\partial h_s}{\partial \boldsymbol{R}_s};$$
(34)

2. the ring-averaged $\boldsymbol{E} \times \boldsymbol{B}$ drift:

$$\left(-\frac{c}{B_0}\frac{\partial \langle\phi\rangle_{\boldsymbol{R}_s}}{\partial \boldsymbol{R}_s} \times \hat{\boldsymbol{z}}\right) \cdot \frac{\partial h_s}{\partial \boldsymbol{R}_s} = \left\langle c\frac{\boldsymbol{E} \times \boldsymbol{B}_0}{B_0^2}\right\rangle_{\boldsymbol{R}_s} \cdot \frac{\partial h_s}{\partial \boldsymbol{R}_s};$$
(35)

3. the ∇B drift:

$$\left(\frac{\partial \langle\boldsymbol{v}_\perp \cdot \boldsymbol{A}_\perp\rangle_{\boldsymbol{R}_s}}{\partial \boldsymbol{R}_s} \times \frac{\hat{\boldsymbol{z}}}{B_0}\right) \cdot \frac{\partial h_s}{\partial \boldsymbol{R}_s} = -\left\langle\frac{\delta B_\parallel}{B_0}\boldsymbol{v}_\perp\right\rangle_{\boldsymbol{R}_s} \cdot \frac{\partial h_s}{\partial \boldsymbol{R}_s},$$
(36)

where, if we expand the ring average (eq. [21]) in small $\boldsymbol{v} \times \hat{\boldsymbol{z}}/\Omega_s$, we get, to lowest order, the familiar drift velocity:

$$-\left\langle\frac{\delta B_\parallel}{B_0}\boldsymbol{v}_\perp\right\rangle_{\boldsymbol{R}_s} \simeq -c\frac{\mu_s \nabla B \times \boldsymbol{B}_0}{q_s B_0^2},$$
(37)

where $\mu_s = m_s v_\perp^2/2B_0$ is the first adiabatic invariant (magnetic moment of the ring) and $\nabla B = \nabla \delta B_\parallel$ is taken at the center of the ring: $\boldsymbol{r} = \boldsymbol{R}_s$;

4. the (linearized) effect of collisions on the perturbed ring distribution function: $-(\partial h_s/\partial t)_{\text{coll}}$ (the gyrokinetic collision operator is discussed in detail in Schekochihin et al. [2006]);

5. the effect of collisionless work done on the rings by the fields (the wave-ring interaction): the right-hand side of equation (29).

We have referred to the ring-averaged versions of the more familiar guiding center drifts. Figure 2 shows the drift of the ring along and across the magnetic field.

2.5. *Heating in Gyrokinetics*

The set of equations given in § 2.4 determines the evolution of the perturbed ring distribution and the field fluctuations on the intermediate timescale characteristic of the turbulent fluctuations. To obtain the evolution of the distribution function F_0 on the slow

---

[7] Note that in the inhomogeneous case, it is more convenient to use the energy $m_s v^2/2$ and the first adiabatic invariant (the magnetic moment) $\mu_s = (1/2)m_s v_\perp^2/B_0$ instead of v and $v_\perp$.

(heating) timescale, we must continue the expansion to order ϵ^2. This is done in Appendix B, where the derivations of the particle transport and heating equations for our homogeneous equilibrium, including the equation defining the conservation of energy in externally driven systems (e.g., "forced" turbulence), are given for the first time. In an inhomogeneous plasma, turbulent diffusion, or transport, also enters at this order and proceeds on the slow timescale. Let us summarize the main results on heating.

In the homogeneous case, there is no particle transport on the slow timescale,

$$\frac{dn_{0s}}{dt} = 0. \quad (38)$$

The evolution of the temperature T_{0s} of species s on this timescale is given by the *heating equation*

$$\frac{3}{2} n_{0s} \frac{dT_{0s}}{dt} = \int d^3\boldsymbol{v} \int \frac{d^3\boldsymbol{R}_s}{V} \overline{q_s \frac{\partial \langle \chi \rangle_{\boldsymbol{R}_s}}{\partial t} h_s} + n_{0s} \nu_E^{sr}(T_{0r} - T_{0s})$$
$$= -\int \frac{d^3\boldsymbol{r}}{V} \int d^3\boldsymbol{v} \, \frac{T_{0s}}{F_{0s}} \overline{\left\langle h_s \left(\frac{\partial h_s}{\partial t}\right)_{\text{coll}} \right\rangle_{\boldsymbol{r}}} + n_{0s} \nu_E^{sr}(T_{0r} - T_{0s}). \quad (39)$$

The overbar denotes the medium-time average over time Δt such that $1/\omega \ll \Delta t \ll 1/(\epsilon^2 \omega)$ (see eq. [B1]). The second term on the right-hand side (proportional to ν_E^{sr}) corresponds to the collisional energy exchange (see, e.g., Helander & Sigmar 2002) between species r and s.[8] It is clear from the second equality in equation (39) that the heating is ultimately always collisional, as it must be, because entropy can only increase due to collisions. When the collisionality is small, $\nu \ll \omega$, the heating is due to the collisionless Landau damping in the sense that the distribution function h_s develops small-scale structure in velocity space, with velocity scales $\Delta \boldsymbol{v} \sim O(\nu^{1/2})$. Collisions smooth these small scales at the rate $\nu v_{\text{th}_i}^2 / (\Delta v)^2 \sim \omega$, so that the heating rate (given by the second expression in eq. [39]) becomes asymptotically independent of ν in the collisionless limit (see related discussion of collisionless dissipation by Krommes & Hu [1994]; Krommes [1999]). We stress that it is essential for any kinetic code, such as GS2, to have some collisions to smooth the velocity distributions at small scales and resolve the entropy production. The numerical demonstration of the collisional heating and its independence of the collision rate is given in § 3.5.

In the homogeneous case, turbulence will damp away unless driven. In our simulations, we study the steady-state homogeneous turbulence driven via an external antenna current $\boldsymbol{j}_a$ introduced into Ampère's law—i.e., the parallel and perpendicular components of $\boldsymbol{j}_a$ are added to the right-hand sides of equations (27) and (28). The work done by the antenna satisfies the *power-balance equation*

$$\int \frac{d^3\boldsymbol{r}}{V} \overline{\boldsymbol{j}_a \cdot \boldsymbol{E}} = \sum_s \int \frac{d^3\boldsymbol{r}}{V} \int d^3\boldsymbol{v} \, \frac{T_{0s}}{F_{0s}} \overline{\left\langle h_s \left(\frac{\partial h_s}{\partial t}\right)_{\text{coll}} \right\rangle_{\boldsymbol{r}}} \quad (40)$$

---

[8] We have been cavalier about treating the collision operator up to this point. The characteristic timescale of the interspecies collisional heat exchange is $\sim \nu^{ii}(m_e/m_i)^{1/2}(T_{0i} - T_{0e})/T_{0e}$. For the two terms on the right-hand side of eq. (39) to be formally of the same order, we must stipulate $\nu^{ii}(m_e/m_i)^{1/2}(T_{0i} - T_{0e})/T_{0e} \sim O(\epsilon^2 \omega)$. This ordering not only ensures that the zeroth-order distribution function is a Maxwellian but also provides greater flexibility in ordering the collisionality relative to the intermediate timescale of the fluctuations. We ignore this technical detail here; in most cases, the second term on the right-hand side of eq. (39) is small compared to the first term, allowing a relatively large temperature difference between species to be maintained.

(see Appendix B.3). Thus, the energy input from the driving antenna is dissipated by heating the plasma species. The lesson of equation (39) is that this heat is always produced by entropy-increasing collisions.

2.6. Linear Collisionless Dispersion Relation

The derivation of the linear dispersion relation from the gyrokinetic equations (25)–(28) is a straightforward linearization procedure. In Appendix C, it is carried out step by step. A key technical fact in this derivation is that once the electromagnetic fields and the gyrokinetic distribution function are expanded in plane waves, the ring averages appearing in the equations can be written as multiplications by Bessel functions. The resulting dispersion relation for linear, collisionless gyrokinetics can be written in the following form,

$$\left(\frac{\alpha_i A}{\overline{\omega}^2} - AB + B^2\right)\left(\frac{2A}{\beta_i} - AD + C^2\right) = (AE + BC)^2, \quad (41)$$

where $\overline{\omega} = \omega/|k_\parallel| v_A$ and, taking $q_i = -q_e = e$, $n_{0i} = n_{0e}$,

$$A = 1 + \Gamma_0(\alpha_i)\xi_i Z(\xi_i) + \frac{T_{0i}}{T_{0e}}[1 + \Gamma_0(\alpha_e)\xi_e Z(\xi_e)], \quad (42)$$

$$B = 1 - \Gamma_0(\alpha_i) + \frac{T_{0i}}{T_{0e}}[1 - \Gamma_0(\alpha_e)], \quad (43)$$

$$C = \Gamma_1(\alpha_i)\xi_i Z(\xi_i) - \Gamma_1(\alpha_e)\xi_e Z(\xi_e), \quad (44)$$

$$D = 2\Gamma_1(\alpha_i)\xi_i Z(\xi_i) + 2\frac{T_{0e}}{T_{0i}}\Gamma_1(\alpha_e)\xi_e Z(\xi_e), \quad (45)$$

$$E = \Gamma_1(\alpha_i) - \Gamma_1(\alpha_e), \quad (46)$$

where $\xi_s = \omega/|k_\parallel| v_{\text{th}_s}$, $Z(\xi_s)$ is the plasma dispersion function, $\alpha_s = k_\perp^2 \rho_s^2/2$, $\Gamma_0(\alpha_s) = I_0(\alpha_s)e^{-\alpha_s}$, and $\Gamma_1(\alpha_s) = [I_0(\alpha_s) - I_1(\alpha_s)]e^{-\alpha_s}$ (I_0 and I_1 are modified Bessel functions). These functions arise from velocity-space integrations and ring averages; see Appendix C for details.

The complex eigenvalue solution $\overline{\omega}$ to equation (41) depends on three dimensionless parameters: the ratio of the ion Larmor radius to the perpendicular wavelength, $k_\perp \rho_i$; the ion plasma β, or the ratio of ion thermal pressure to magnetic pressure, β_i; and the ion to electron temperature ratio, T_{0i}/T_{0e}. Thus, $\overline{\omega} = \overline{\omega}_{\text{GK}}(k_\perp \rho_i, \beta_i, T_{0i}/T_{0e})$.

2.6.1. Long-Wavelength Limit

Let us first consider the linear physics at scales large compared to the ion Larmor radius, for which the comparison to MHD is more straightforward. These are not new results, but they are an important starting point for the more general results to follow. First, recall the MHD waves in the anisotropic limit $k_\parallel \ll k_\perp$:

$$\omega = \pm k_\parallel v_A, \qquad \text{Alfvén waves}, \quad (47)$$

$$\omega \simeq \pm \frac{k_\parallel v_A}{\sqrt{1 + v_A^2/c_s^2}}, \quad \text{slow waves}, \quad (48)$$

$$\omega \simeq \pm k_\perp \sqrt{c_s^2 + v_A^2}, \quad \text{fast magnetosonic waves}, \quad (49)$$

$$\omega = 0, \qquad \text{entropy mode}, \quad (50)$$

where c_s is the sound speed. The fast magnetosonic waves have been ordered out of gyrokinetics because, when $k_\perp \rho_i \sim 1$, their frequency is of order the cyclotron frequency Ω_i. The removal of the fast waves is achieved by balancing the perpendicular

plasma pressure with the magnetic field pressure (see eq. [A30]). Here we are concerned with the Alfvén and slow waves in the collisionless limit. Note that the entropy mode is mixed with the slow-wave mode when the parallel wavelength is below the ion mean free path. In this paper, whenever we refer to the "slow-wave" part of the dispersion relation, we sacrifice terminological precision to brevity. Strictly speaking, the slow waves, as understood below, are everything that is not Alfvén waves, namely, modes involving fluctuations of the magnetic field strength, which can also be aperiodic (have zero real frequency) (for further discussion of this component of gyrokinetic turbulence, see Schekochihin et al. [2006]).

The left-hand side of equation (41) contains two factors. We see that the first factor corresponds to the Alfvén wave solution, the second to the slow-wave solution. The right-hand side of equation (41) represents the coupling between the Alfvén and slow waves that is only important at finite ion Larmor radius.

In the long-wavelength limit $k_\perp \rho_i \ll 1$, or $\alpha_i \ll 1$, we can expand $\Gamma_0(\alpha_s) \simeq 1 - \alpha_s$ and $\Gamma_1(\alpha_s) \simeq 1 - 3\alpha_s/2$. We can also neglect terms that multiply powers of the electron-ion mass ratio, m_e/m_i, a small parameter. In this limit, $B \simeq \alpha_i$, $E \simeq -(3/2)\alpha_i$, and the dispersion relation simplifies to

$$\left(\frac{1}{\omega^2} - 1\right)\left(\frac{2A}{\beta_i} - AD + C^2\right) = 0. \quad (51)$$

The first factor leads to the familiar Alfvén-wave dispersion relation:

$$\omega = \pm k_\parallel v_A. \quad (52)$$

It is not hard to verify that this branch corresponds to fluctuations of ϕ and $A_\parallel$, but not of $\delta B_\parallel$. Thus, the Alfvén-wave dispersion relation in the $k_\perp \rho_i \to 0$ limit is unchanged from the MHD result. This is expected (and well known) since this wave involves no motions or forces parallel to the mean magnetic field. The wave is undamped, and the plasma dispersion function (which contains the wave-particle resonance effects) does not appear in this branch of the dispersion relation. To higher order in $k_\perp \rho_i$, however, the Alfvén wave is weakly damped; taking the high-β result ($\beta_i \gg 1$), derived in Appendix D.1, the damping of the Alfvén wave in the limit $k_\perp \rho_i \ll 1$ is

$$\gamma = -|k_\parallel| v_A \frac{9}{16} \frac{k_\perp^2 \rho_i^2}{2} \sqrt{\frac{\beta_i}{\pi}}. \quad (53)$$

The second factor in equation (51) represents the slow-wave solution of the dispersion relation. This involves motions and forces along the magnetic field line (perturbations of $\delta B_\parallel$, but not of $A_\parallel$) and, unlike in the MHD collisional limit, is damped significantly (Barnes 1966; Foote & Kulsrud 1979). The plasma dispersion function enters through A, C, and D; to further simplify the expression for the slow wave, we consider the high- and low-β limits.

In the high-β limit, $\beta_i \gg 1$, the argument of the plasma dispersion function for the ion terms will be small, $\xi_i = \overline{\omega}/\beta_i^{1/2} \sim O(1/\beta_i)$ (verified by the outcome), and we can use the power series expansion (Fried & Conte 1961)

$$\xi_i Z(\xi_i) \simeq i\sqrt{\pi}\xi_i - 2\xi_i^2 \quad (54)$$

to solve for the complex frequency analytically. The electron terms may be dropped because $\xi_e = \xi_i(T_{0i}/T_{0e})^{1/2}(m_e/m_i)^{1/2} \ll \xi_i$.

Then we can approximate $A \simeq 1 + T_{0i}/T_{0e}$, $C \simeq i\sqrt{\pi}\xi_i$, and $D \simeq 2\sqrt{\pi}\xi_i$. The dispersion relation reduces to

$$\frac{2}{\beta_i} - D = 0, \quad (55)$$

whose solution is $\xi_i = -i/\sqrt{\pi}\beta_i$, or

$$\omega = -i\frac{|k_\parallel| v_A}{\sqrt{\pi\beta_i}}. \quad (56)$$

This frequency is purely imaginary, so the mode does not propagate and is strictly damped, in agreement with Foote & Kulsrud (1979). Note that $\xi_i \sim O(1/\beta_i)$, confirming the a priori assumption used to derived this result.

In the low-β limit, $\beta_i \ll 1$, we shall see that the phase velocity of the slow wave is of the order of the sound speed $c_s = (T_{0e}/m_i)^{1/2}$. The electrons then move faster than the wave, and we can drop all terms involving electron plasma dispersion functions because $\xi_e \sim c_s/v_{th_e} = (m_e/2m_i)^{1/2} \ll 1$. If we further assume that $T_{0e} \gg T_{0i}$, then the ions are moving slower than the sound speed, so we have $\xi_i \sim c_s/v_{th_i} = (T_{0e}/2T_{0i})^{1/2} \gg 1$. Expanding the plasma dispersion function in this limit gives (Fried & Conte 1961)

$$\xi_i Z(\xi_i) \simeq i\sqrt{\pi}\xi_i e^{-\xi_i^2} - 1 - \frac{1}{2\xi_i^2}. \quad (57)$$

Using this expansion in $A \simeq 1 + \xi_i Z(\xi_i) + T_{0i}/T_{0e}$, $C \simeq \xi_i Z(\xi_i)$, and $D \simeq 2\xi_i Z(\xi_i)$, we find that the slow-wave part of equation (51) now reduces to $A = 0$, or

$$\frac{T_{0i}}{T_{0e}} - \frac{1}{2}\left(\frac{k_\parallel v_{th_i}}{\omega}\right)^2 + i\sqrt{\pi}\frac{\omega}{|k_\parallel| v_{th_i}}e^{-(\omega/k_\parallel v_{th_i})^2} = 0. \quad (58)$$

Assuming weak damping, to be checked later, we can solve for the real frequency and damping rate by expanding this equation about the real frequency. Solving for the real frequency from the real part of equation (58) gives

$$\omega = \pm k_\parallel c_s. \quad (59)$$

This is the familiar ion acoustic wave. Solving for the damping gives

$$\gamma = -|k_\parallel| c_s \sqrt{\frac{\pi}{8}}\left(\frac{T_{0e}}{T_{0i}}\right)^{3/2} e^{-T_{0e}/2T_{0i}}. \quad (60)$$

This solution agrees with the standard solution for ion acoustic waves (see, e.g., § 8.6.3 of Krall & Trivelpiece 1986) in the limit $k^2\lambda_{De}^2 \ll 1$. Note that the a priori assumptions we made above are verified by this result.

In summary, the gyrokinetic dispersion relation in the long-wavelength limit, $k_\perp \rho_i \ll 1$, separates neatly into an Alfvén wave mode and a slow-wave mode, while the fast wave is ordered out by the gyrokinetic approximation. We have seen here that slow waves are subject to collisionless Landau damping, even in the long-wavelength limit, $k_\perp \rho_i \ll 1$. Therefore, if the scale of turbulent motions falls below the mean free path, the slow mode should be effectively damped out, particularly for high-β plasmas. In contrast, the Alfvén waves are undamped down to scales around the ion Larmor radius. The linear damping of the Alfvén waves at these scales is worked out in Appendices D1 and D2, where we

present the high- and low-β limits, respectively, of the gyrokinetic dispersion relation including the effects associated with the finite Larmor radius. The nature of the turbulent cascades of Alfvén and slow waves at collisionless scales is discussed in more detail in Schekochihin et al. (2006).

2.6.2. *Short-Wavelength Limit*

At wavelengths small compared to the ion Larmor radius, $k_\perp \rho_i \gg 1$, the low-frequency dynamics are those of kinetic Alfvén waves. It is expected that, while the Alfvén wave cascade is damped around $k_\perp \rho_i \sim 1$, some fraction of the Alfvén wave energy seeps through to wavelengths smaller than the ion Larmor radius and is channeled into a cascade of kinetic Alfvén waves. This cascade extends to yet smaller wavelengths until the electron Larmor radius is reached, $k_\perp \rho_e \sim 1$, at which point the kinetic Alfvén waves Landau damp on the electrons.

In the limit $k_\perp \rho_i \gg 1$, $k_\perp \rho_e \ll 1$, we have $\Gamma_0(\alpha_i)$, $\Gamma_1(\alpha_i) \to 0$ and $\Gamma_0(\alpha_e) \simeq \Gamma_1(\alpha_e) \simeq 1$, whence $B \simeq 1$, and $E \simeq -1$. We assume a priori and verify below that $\xi_e \sim O(k_\perp \rho_e) \ll 1$, so the electron plasma dispersion functions may be dropped to lowest order in $k_\perp \rho_e$. The gyrokinetic dispersion relation is then

$$\left(\frac{\alpha_i A}{\overline{\omega}^2} - A + 1 \right) \frac{2}{\beta_i} = A, \tag{61}$$

where $A \simeq 1 + T_{0i}/T_{0e}$. The solution is

$$\omega = \pm \frac{k_\parallel v_A k_\perp \rho_i}{\sqrt{\beta_i + 2/(1 + T_{0e}/T_{0i})}}. \tag{62}$$

This agrees with the kinetic Alfvén wave dispersion relation derived in the general plasma setting (see, e.g., Kingsep et al. 1990). Note that, for this solution, $\xi_e \sim O(k_\perp \rho_e)$ as promised.

In order to get the (small) damping decrement of these waves, we retain the electron plasma dispersion functions: these are approximated by $Z(\xi_e) \simeq i\sqrt{\pi}$. Then $A \simeq 1 + (T_{0i}/T_{0e})(1 + i\sqrt{\pi}\xi_e)$, $C \simeq -i\sqrt{\pi}\xi_e$, and $D \simeq i2(T_{0e}/T_{0i})\sqrt{\pi}\xi_e$. Expanding the resulting dispersion relation around the lowest order solution (eq. [62]), we get

$$\gamma = -i|k_\parallel| v_A \frac{k_\perp^2 \rho_i^2}{2} \left(\frac{\pi}{\beta_i} \frac{T_{0e}}{T_{0i}} \frac{m_e}{m_i} \right)^{1/2}$$
$$\times \left\{ 1 - \frac{1}{2} \frac{1 + (1 + T_{0e}/T_{0i})\beta_i}{[1 + (1 + T_{0e}/T_{0i})\beta_i/2]^2} \right\}. \tag{63}$$

The transition between the long-wavelength solutions of § 2.6.1 and the short-wavelength ones of this section is treated (in the analytically tractable limits of high and low β_i) in Appendices D1 and D2.

3. NUMERICAL TESTS

Gyrokinetic theory is a powerful tool for investigating nonlinear, low-frequency kinetic physics. This section presents the results of a suite of linear tests over a wide range of the three relevant parameters: the ratio of the ion Larmor radius to the perpendicular wavelength, $k_\perp \rho_i$; the ion plasma β, or the ratio of ion thermal pressure to magnetic pressure, β_i; and the ion to electron temperature ratio, T_{0i}/T_{0e}. We compare the results of three numerical methods: the gyrokinetic simulation code GS2, the linear collisionless gyrokinetic dispersion relation, and the linear hot-plasma dispersion relation.

For a wide range of parameters, we present three tests of the code for verification: § 3.2 presents the frequency and damping rate of Alfvén waves, § 3.3 compares the ratio of ion to electron heating due to the linear collisionless damping of Alfvén waves, and § 3.4 examines the density fluctuations associated with the Alfvén mode when it couples to the compressional slow wave around $k_\perp \rho_i \sim O(1)$. The effect of collisions on the collisionless damping rates is discussed in § 3.5. The breakdown of gyrokinetic theory in the limit of weak anisotropy $k_\parallel \sim k_\perp$ and high frequency $\omega \sim \Omega_i$ is demonstrated and discussed in § 3.6.

3.1. *Technical Details*

GS2 is a publicly available, widely used gyrokinetic simulation code, developed[9] to study low-frequency turbulence in magnetized plasmas (Kotschenreuther et al. 1995; Dorland et al. 2000). The basic algorithm is Eulerian; equations (25)–(28) are solved for the self-consistent evolution of five-dimensional distribution functions (one for each species) and the electromagnetic fields on fixed spatial grids. All linear terms are treated implicitly, including the field equations. The nonlinear terms are advanced with an explicit, second-order accurate, Adams-Bashforth scheme.

Since turbulent structures in gyrokinetics are highly elongated along the magnetic field, GS2 uses field line–following Clebsch coordinates to resolve such structures with maximal efficiency, in a flux tube of modest perpendicular extent (Beer et al. 1995). Pseudospectral algorithms are used in the spatial directions perpendicular to the field and for the two velocity space coordinate grids (energy $v^2/2$ and magnetic moment $v_\perp^2/2B$) for high accuracy on computable five-dimensional grids. The code offers wide flexibility in simulation geometry, allowing for optimal representation of the complex toroidal geometries of interest in fusion research. For the astrophysical applications pursued here, we require only the simple, periodic-slab geometry in a uniform equilibrium magnetic field with no mean temperature or density gradients.

The linear calculations of collisionless wave damping and particle heating presented in this section employed an antenna driving the parallel component of the vector potential $A_\parallel$ (this drives a perpendicular perturbation of the magnetic field). The simulation was driven at a given frequency ω_a and wavenumber $\boldsymbol{k}_a$ by adding an external current $j_{\parallel a}$ into the parallel Ampère's law (eq. [27]). To determine the mode frequency ω and damping rate γ, the driving frequency was swept slowly ($\dot{\omega}_a/\omega_a \ll \gamma$) through the resonant frequency to measure the Lorentzian response. Fitting the curve of the Lorentzian recovers the mode frequency and damping rate. These damping rates were verified in decaying runs: the plasma was driven to steady state at the resonant frequency $\omega_a = \omega$; then the antenna was shut off and the decay rate of the wave energy measured.

The ion-to-electron heating ratio was determined by driving the plasma to steady state at the resonant frequency $\omega_a = \omega$ and calculating the heating of each species using diagnostics based on both forms of the heating equation (39). In all methods, a realistic mass ratio is used assuming a hydrogenic plasma. The linear GS2 runs used a single $k_\perp$ mode and 16 points in the parallel direction. For most runs a velocity space resolution of 20×16 points was adequate; the ion and electron heating ratio runs required higher velocity space resolution to resolve the heating of the weakly damped species, with extreme cases requiring up to 80×40 points in velocity space.
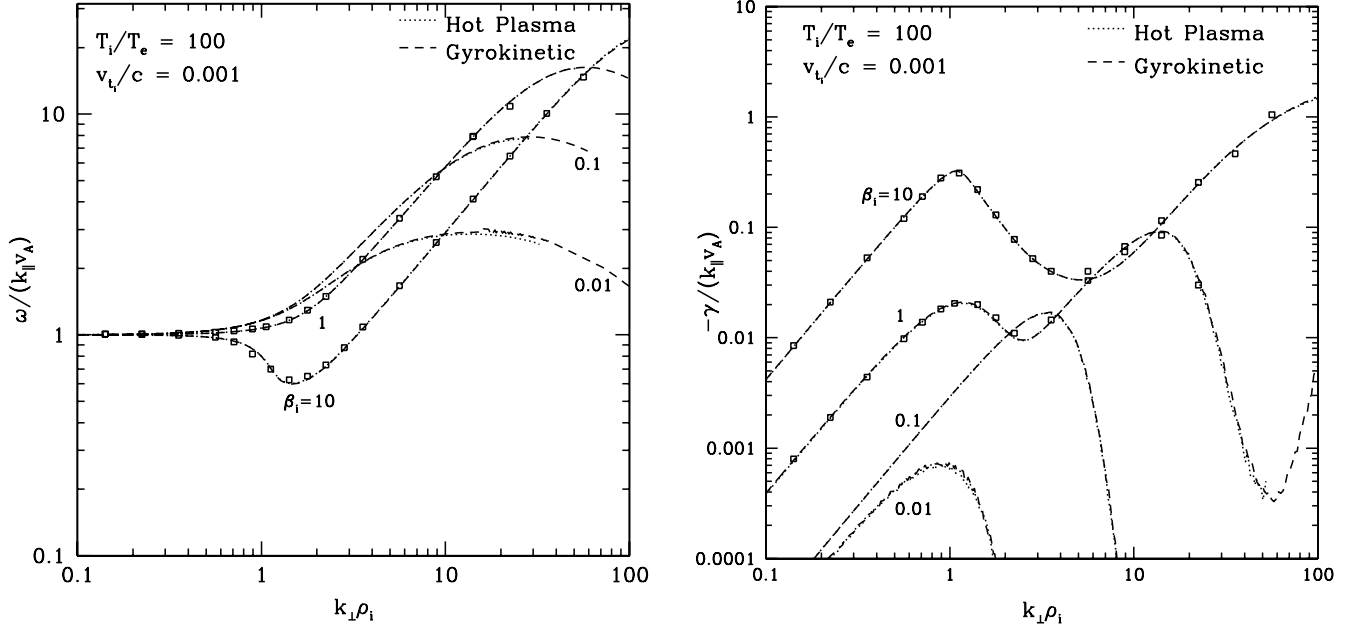
Fig. 3.—Normalized real frequency $\omega/k_\parallel v_A$ (*left*) and damping rate $\gamma/k_\parallel v_A$ (*right*) vs. $k_\perp \rho_i$ for a temperature ratio $T_{0i}/T_{0e} = 100$ and ion plasma β-values $\beta_i = 10$, 1, 0.1, and 0.01. Plotted are numerical solutions to the gyrokinetic dispersion relation (*dashed lines*), numerical solutions to the hot-plasma dispersion relation (*dotted lines*), and results from the GS2 gyrokinetic code (*squares*).

In what follows, the linear results obtained from GS2 are compared to two sets of analytical solutions:

1. Given the three input parameters $k_\perp \rho_i$, β_i, and T_{0i}/T_{0e}, the linear, collisionless gyrokinetic dispersion relation (eq. [41]) is solved numerically using a two-dimensional Newton's method root search in the complex frequency plane, obtaining the solution $\overline{\omega} = \overline{\omega}_{GK}(k_\perp \rho_i, \beta_i, T_{0i}/T_{0e})$.

2. The hot-plasma dispersion relation (see, e.g., Stix 1992) is solved numerically (also using a two-dimensional Newton's method root search) for an electron and proton plasma characterized by an isotropic Maxwellian with no drift velocities (Quataert 1998). To obtain accurate results at high $k_\perp \rho_i$, it is necessary that the number of terms kept in the sums of Bessel functions appearing in the hot-plasma dispersion relation is about the same as $k_\perp \rho_i$. The linear hot-plasma dispersion relation depends on five parameters: $k_\perp \rho_i$, the ion plasma beta β_i, the ion to electron temperature ratio T_{0i}/T_{0e}, the ratio of the parallel to the perpendicular wavelength $k_\parallel/k_\perp$, and the ratio of the ion thermal velocity to the speed of light v_{th_i}/c. Hence, the solution may be expressed as $\overline{\omega} = \overline{\omega}_{HP}(k_\perp \rho_i, \beta_i, T_{0i}/T_{0e}, k_\parallel/k_\perp, v_{\mathrm{th}_i}/c)$. The hot-plasma theory must reduce to gyrokinetic theory in the limit of $k_\parallel \ll k_\perp$ and $v_{\mathrm{th}_i}/c \ll 1$, i.e., $\overline{\omega}_{HP}(k_\perp \rho_i, \beta_i, T_{0i}/T_{0e}, 0, 0) = \overline{\omega}_{GK}(k_\perp \rho_i, \beta_i, T_{0i}/T_{0e})$.

3.2. *Frequency and Damping Rates*

The frequency and collisionless damping rates for the three methods are compared for temperature ratios $T_{0i}/T_{0e} = 100$ and 1 and for ion plasma β-values $\beta_i = 10$, 1, 0.1, and 0.01 over a range of $k_\perp \rho_i$ from 0.1 to 100. The temperature ratio $T_{0i}/T_{0e} = 100$ is motivated by accretion disk physics, and the temperature ratio $T_{0i}/T_{0e} = 1$ is appropriate for studies of the interstellar medium and the solar wind. The real frequency ω and the damping rate γ are normalized to the Alfvén frequency $k_\parallel v_A$. The hot-plasma calculations in this section all have $k_\parallel/k_\perp = 0.001$ and $v_{\mathrm{th}_i}/c = 0.001$. The number of Bessel functions used in the sum for these results was 100, so the results will be accurate for $k_\perp \rho_i \lesssim 100$.

Figure 3 presents the results for the temperature ratio $T_{0i}/T_{0e} = 100$, and Figure 4 presents those for the temperature ratio $T_{0i}/T_{0e} = 1$. The results confirm accurate performance by GS2 over the range of parameters tested.

3.3. *Ion and Electron Heating*

An important goal of our nonlinear gyrokinetic simulations to be presented in future papers is to calculate the ratio of ion to electron heating in collisionless turbulence (motivated by issues that arise in the physics of accretion disks; see Quataert [1998]; Quataert & Gruzinov [1999]). Using the heating equation (39), the solutions of the linear collisionless dispersion relation can be used to calculate the heat deposited into the ions and electrons for a given linear wave mode. These results for ion to electron power are verified against estimates of the heating from the hot-plasma dispersion relation and compared to numerical results from GS2 in Figure 5. The power deposited into each species P_s is calculated by GS2 using both forms of the heating equation (39) (neglecting interspecies collisions). Here we have plotted the ion to electron power for a temperature ratio of $T_{0i}/T_{0e} = 100$ and ion plasma β values of $\beta_i = 1$ and 10. The GS2 results agree well with the linear gyrokinetic and linear hot-plasma calculations over 5 orders of magnitude in the power ratio.

3.4. *Density Fluctuations*

Alfvén waves in the MHD limit (at large scales) are incompressible, with no motion along the magnetic field and no associated density fluctuations. However, as Alfvén waves nonlinearly cascade to small scales and reach $k_\perp \rho_i \sim 1$, finite Larmor radius effects give rise to nonzero parallel motions, driving density fluctuations. Here we compare the density fluctuations predicted by the linear gyrokinetic dispersion relation with that from hot-plasma theory. Figure 6 compares the density fluctuations for a plasma with temperature ratio $T_{0i}/T_{0e} = 1$ and values of ion plasma $\beta_i = 0.1$, 1, and 10, parameter values relevant to the observations of interstellar scintillation in the interstellar medium. These results demonstrate that the fractional electron density fluctuations
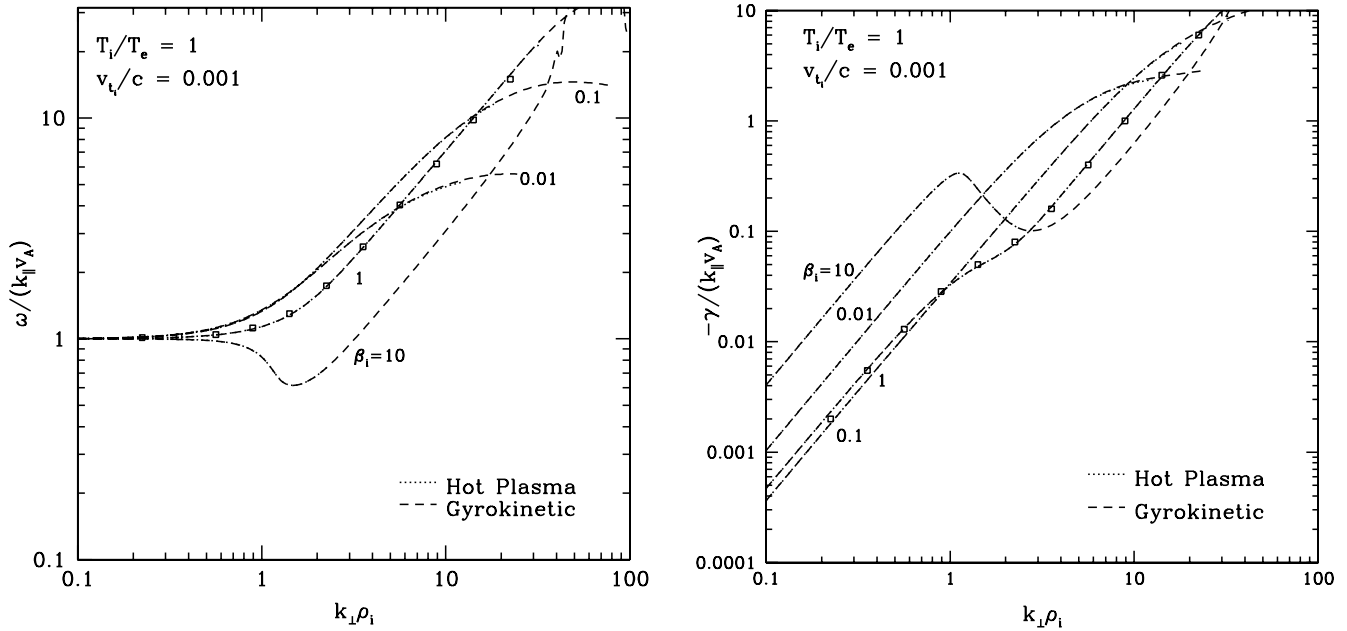
Fig. 4.—Same as Fig. 3, but for $T_{0i}/T_{0e} = 1$.

$|\delta n_{0e}|/n_{0e}$, normalized by the electron velocity fluctuation, peak near the ion Larmor radius as expected.

3.5. Collisions

Gyrokinetic theory is valid in both the collisionless and collisional limits. To demonstrate the effect of collisionality, implemented in GS2 using a pitch-angle scattering operator on each species with a coefficient ν_s, Figure 7 presents the measured linear damping rate in GS2 as the collision rate is increased. Parameters for this demonstration are $\beta_i = 10$, $T_{0i}/T_{0e} = 100$, and $k_\perp \rho_i = $

1.414. The collision rates for both species are set to be equal, $\nu = \nu_{ii} = \nu_{ee}$, and interspecies collisions are turned off. The figure clearly demonstrates that in the collisionless limit, $\nu \ll \omega$, the damping rate due to collisionless processes becomes independent of ν. As the collision rate is increased, heating via collisionless Landau damping becomes less effective, and the measured damping rate decreases; this is expected because, in the MHD limit where collisions dominate, Alfvén waves are undamped. As discussed in § 2.5, however, all heating is ultimately collisional because collisions are necessary to smooth
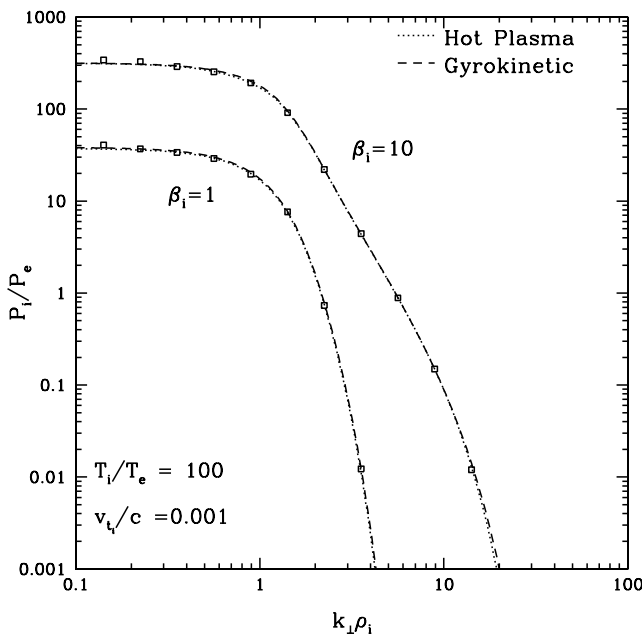

Fig. 5.—Ratio of the ion to electron heating P_i/P_e. Results are shown for a temperature ratio of $T_{0i}/T_{0e} = 100$ and values of ion plasma beta $\beta_i = 1$ and 10. Plotted are derived values using the gyrokinetic dispersion relation (*dashed lines*) and the hot-plasma dispersion relation (*dotted lines*); results from the GS2 gyrokinetic initial value code show good agreement over nearly 5 orders of magnitude (*squares*).
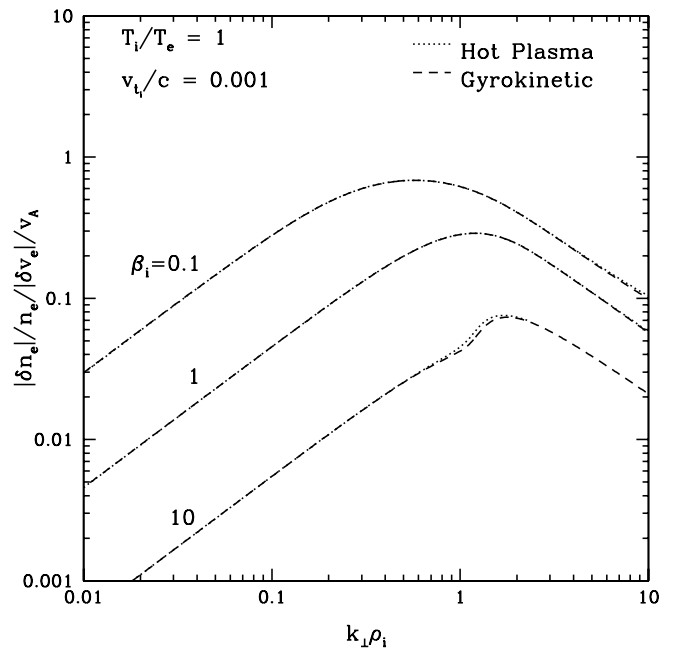
Fig. 6.—Electron density fluctuations for a plasma with a temperature ratio of $T_{0i}/T_{0e} = 1$ and values of ion plasma beta $\beta_i = 0.1$, 1, and 10 using the gyrokinetic dispersion relation (*dashed lines*) and the hot-plasma dispersion relation (*dotted lines*). The fractional electron density fluctuation $|\delta n_e|/n_{0e}$ is normalized here by the total electron velocity fluctuations relative to the Alfvén speed $|\delta v_e|/v_A$.
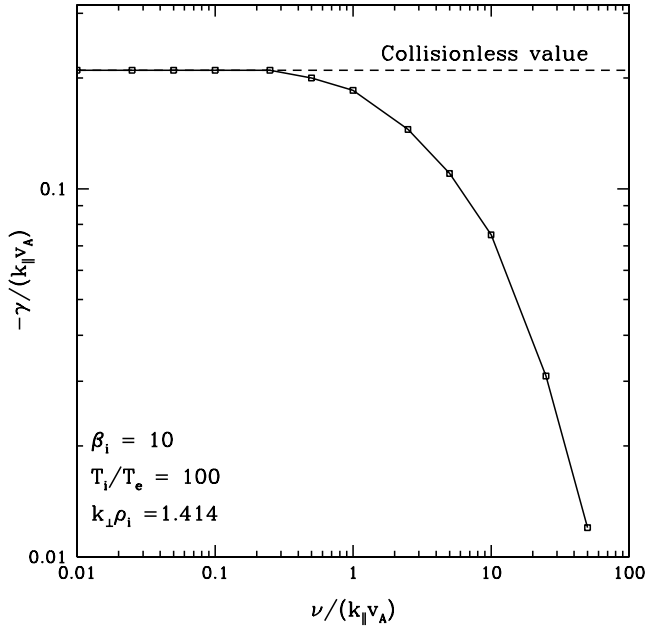
Fig. 7.—Damping rate γ determined in linear runs of GS2 (*squares*) vs. the collision rate ν normalized by $k_\| v_A$. In the collisionless limit, $\nu \ll \omega$, the damping rate is independent of the collision rate as expected. As the collision rate is increased, collisionless processes for damping the wave are less effective, and the damping rate diminishes.
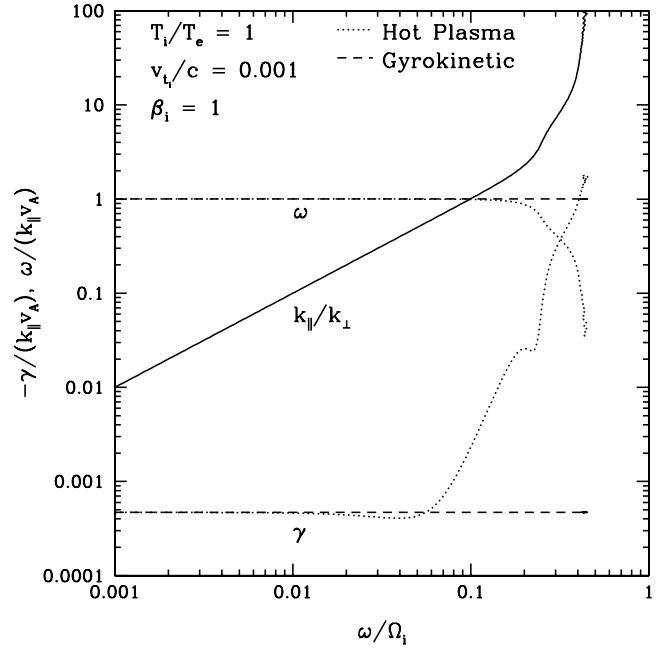

Fig. 8.—For a plasma with $T_{0i}/T_{0e} = 1$, $\beta_i = 1$, and $k_\perp \rho_i = 0.1$, limits of applicability of the gyrokinetic solution (*dashed line*) as the latter deviates from the hot-plasma solution (*dotted line*) when $\omega/\Omega_i \to 1$. Also plotted (*solid line*) is the value of $k_\|/k_\perp$ as a function of ω/Ω_i.

out the small-scale structure in velocity space produced by wave-particle interactions. A minimum collision rate must be specified for the determination of the heating rate to converge. In the low velocity space resolution runs (10×8 in velocity space) presented in Figure 7, for $\nu/(k_\| v_A) < 0.01$, the heating rate did not converge accurately. Increasing the velocity-space resolution lowers the minimum threshold on the collision rate necessary to achieve convergence.

3.6. *Limits of Applicability*

The gyrokinetic theory derived here is valid as long as three important conditions are satisfied: (1) $k_\| \ll k_\perp$, (2) $\omega \ll \Omega_i$, and (3) $v_{th_s} \ll c$ (the nonrelativistic assumption is not essential, but it is adopted in our derivation). As discussed at the end of § 2.1, the gyrokinetic formalism retains the low-frequency dynamics of the slow and Alfvén waves and collisionless dissipation via the Landau resonance but orders out the higher frequency dynamics of the fast MHD wave and cyclotron resonances.

A demonstration of the breakdown of the gyrokinetic approximation when these limits are exceeded is provided in Figure 8 for a plasma with $T_{0i}/T_{0e} = 1$, $\beta_i = 1$, and $k_\perp \rho_i = 0.1$. Here, we increase the ratio of the parallel to perpendicular wavenumber $k_\|/k_\perp$ from 0.001 to 100 and solve for the frequency using the hot-plasma dispersion relation. The frequency increases toward the ion cyclotron frequency as the wavenumber ratio approaches unity. The frequency $\omega/k_\| v_A$ in gyrokinetics is independent of the value of $k_\|$, so we compare these gyrokinetic values with the hot-plasma solution. Figure 8 plots the normalized real frequency $\omega/k_\| v_A$ and damping rate $|\gamma|/k_\| v_A$ against the ratio of the real frequency to the ion cyclotron frequency ω/Ω_i. Also plotted is the value of $k_\|/k_\perp$ at each ω/Ω_i. At $\omega/\Omega_i \sim 0.01$ and $k_\|/k_\perp \sim 0.1$, the damping rate deviates from the gyrokinetic solution as cyclotron damping becomes important. The real frequency departs from the gyrokinetic results at $\omega/\Omega_i \sim 0.1$ and $k_\|/k_\perp \sim 1$. It is evident that gyrokinetic theory gives remarkably good results even when $k_\|/k_\perp \sim 0.1$.

4. CONCLUSION

This paper is the first in a series to study the properties of low-frequency anisotropic turbulence in collisionless astrophysical plasmas using gyrokinetics. Our primary motivation for investigating this problem is that such turbulence appears to be a natural outcome of MHD turbulence as energy cascades to small scales nearly perpendicular to the direction of the local magnetic field (see Fig. 1). Gyrokinetic turbulence may thus be a generic feature of turbulent astrophysical plasmas.

Gyrokinetics is an approximation to the full theory of collisionless and collisional plasmas. The necessary assumptions are that turbulent fluctuations are anisotropic with parallel wavenumbers small compared to perpendicular wavenumbers, $k_\| \ll k_\perp$, that frequencies are small compared to the ion cyclotron frequency, $\omega \ll \Omega_i$, and that fluctuations are small so that the typical plasma or field line displacement is of order $O(k_\perp^{-1})$. In this limit, one can average over the Larmor motion of particles, simplifying the dynamics considerably. Although gyrokinetics assumes $\omega \ll \Omega_i$, it allows for $k_\perp \rho_i \sim 1$, i.e., wavelengths in the direction perpendicular to the magnetic field can be comparable to the ion Larmor radius. On scales $k_\perp \rho_i \lesssim 1$, the gyrokinetic approximation orders out the fast MHD wave but retains the slow wave and the Alfvén wave. Gyrokinetics also orders out cyclotron-frequency effects such as the cyclotron resonant heating but retains collisionless damping via the Landau resonance.[10] It is worth noting that reconnection in the presence of a strong guide field can be described by gyrokinetics, so the current sheets that develop on scales of less than or equal to ρ_i in a turbulent plasma are self-consistently modeled in a nonlinear gyrokinetic simulation. The enormous value of gyrokinetics as an approximation is threefold: first, it considerably simplifies the linear and nonlinear equations; second, it removes the fast cyclotron timescales and the gyrophase

---

[10] We are describing here the standard version of gyrokinetics. See Qin et al. (2000) for an extended theory that includes the fast-wave and high-frequency modes.

angle dimension of the phase space; and third, it allows for a simple physical interpretation in terms of the motion of charged rings.

In this paper, we have presented a derivation of the gyrokinetic equations, including, for the first time, the equations describing particle heating and global energy conservation. The dispersion relation for linear collisionless gyrokinetics is derived and its physical interpretation is discussed. At scales $k_\perp \rho_i \ll 1$, the familiar MHD Alfvén and slow modes are recovered. As scales such that $k_\perp \rho_i \sim 1$ are approached, there is a linear mixing of the Alfvén and slow modes. This leads to effects such as collisionless damping of the Alfvén wave and finite-density fluctuations in linear Alfvén waves. We have compared the gyrokinetic results with those of hot-plasma kinetic theory, showing the robustness of the gyrokinetic approximation. We also used comparisons with the analytical results from both theories to verify and demonstrate the accuracy of the gyrokinetic simulation code GS2 in the parameter regimes of astrophysical interest. We note that although our tests are linear, GS2 has already been used extensively for nonlinear turbulence problems in the fusion research (e.g., Dorland et al. 2000; Jenko et al. 2000, 2001; Rogers et al. 2000; Jenko & Dorland 2001, 2002; Candy et al. 2004; Ernst et al. 2004), and a program of nonlinear astrophysical turbulence simulations is currently underway.

In conclusion, we briefly mention some of the astrophysics problems that will be explored in more detail in our future work:

1. Energy in Alfvénic turbulence is weakly damped until it cascades to $k_\perp \rho_i \sim 1$. Thus, gyrokinetics can be used to calculate the species by species heating of plasmas by low-frequency MHD turbulence in which the dominant heating is due to the Landau resonance. In future work, we will carry out gyrokinetic turbulent heating calculations and apply them to particle heating in solar flares, the solar wind, and hot radiatively inefficient accretion flows (see Quataert 1998; Gruzinov 1998; Quataert & Gruzinov 1999; Leamon et al. 1998, 1999, 2000; Cranmer & van Ballegooijen 2003, 2005, for related analytical and observational results). The use of the gyrokinetic formalism, which orders out high-frequency dynamics, such as fast MHD waves and cyclotron heating, is justified on the assumption that the turbulent cascade remains highly anisotropic down to scales of order ion Larmor radius, so that the fluctuation frequencies are well below the cyclotron frequency even when $k_\perp \rho_i \sim 1$, rendering the cyclotron resonance unimportant to the plasma heating.

2. In situ observations of the turbulent solar wind directly measure the power spectra of the magnetic field (Goldstein et al. 1995; Leamon et al. 1998, 1999) and the electric field (Bale et al. 2005) down to scales smaller than the ion gyroradius. Thus, detailed quantitative comparisons between simulated power spectra and the measured ones are possible. It is worth noting, however, that the solar wind is, in fact, sufficiently collisionless that the gyrokinetic ordering here is not entirely appropriate and the equilibrium distribution function F_0 may deviate from a Maxwellian. Significant distortions of F_0, however, are tempered by high-frequency kinetic mirror and firehose instabilities that may play the role of collisions in smoothing out the distribution function, so the solar wind plasma may not depart significantly from gyrokinetic behavior. It must be kept in mind, however, that if these instabilities were effective in driving a cascade to higher $k_\parallel$ (and thus higher frequency), the gyrokinetic approximation would be violated and further analysis required to take account of the small-scale physics.

3. In the interstellar medium of the Milky Way, the electron-density fluctuation power spectrum, inferred from observations, is consistent with Kolmogorov turbulence over 10 decades in spatial scale (see Armstrong et al. 1995). Observations suggest the existence of an inner scale to the density fluctuations at approximately the ion Larmor radius (Spangler & Gwinn 1990). These observations may be probing the density fluctuations associated with Alfvén waves on gyrokinetic scales (see § 3.4)—precisely the regime that is best investigated by gyrokinetic simulations.

APPENDIX A

DERIVATION OF THE GYROKINETIC EQUATIONS

The nonlinear gyrokinetic equation in an inhomogeneous plasma was first derived by Frieman & Chen (1982). In this appendix, we derive the nonlinear gyrokinetic equation in the simplest case in which the equilibrium is a homogeneous plasma in a constant magnetic field, i.e., $\nabla F_0 = 0$ and $\boldsymbol{B}_0 = B_0 \hat{\boldsymbol{z}}$ in a periodic box. We begin with the Fokker-Planck equation and Maxwell's equations. The gyrokinetic ordering, which makes the expansion procedure possible, was explained in § 2.1. The guiding center coordinates and the key mathematical operation, ring averaging, were introduced in § 2.3. In what follows, the Fokker-Planck equation is systematically expanded under the gyrokinetic ordering. The minus first, zeroth, and first orders are solved to determine both the form of the equilibrium distribution function and the evolution equation for the perturbed distribution function, the gyrokinetic equation (the slow evolution of the equilibrium enters in the second order and is worked out in Appendix B). At each order, a ring average at constant guiding center position is employed to eliminate higher orders from the equation. Velocity integration of the perturbed distribution function yields the charge and current densities that appear in the gyrokinetic versions of Maxwell's equations.

A1. MAXWELL'S EQUATIONS AND POTENTIALS

Let us start with Poisson's law. The equilibrium plasma is neutral, $\sum_s q_s n_{0s} = 0$, so we have

$$\nabla \cdot \delta \boldsymbol{E} = 4\pi \sum_s q_s \delta n_s. \tag{A1}$$

The left-hand side is $O(\epsilon B_0 v_{\mathrm{th}_i}/c\rho_i)$ (see eq. [8]), and the right-hand side is $O(\epsilon q_i n_{0i})$, so the ratio of the divergence of the electric field to the charge density is $O(\beta_i^{-1} v_{\mathrm{th}_i}^2/c^2)$. Therefore, in the limit of nonrelativistic ions, the perturbed charge density is zero.[11] This establishes the condition of quasineutrality:

$$\sum_s q_s \delta n_s = 0. \tag{A2}$$

In Faraday's law,

$$c\nabla \times \delta\boldsymbol{E} = -\frac{\partial \delta\boldsymbol{B}}{\partial t}; \tag{A3}$$

the left-hand side is $O(\epsilon\Omega_i B_0)$, whereas the right-hand side is $O(\epsilon^2 \Omega_i B_0)$. Therefore, to dominant order the electric field satisfies $\nabla \times \delta\boldsymbol{E} = 0$, so the largest part of the electric field is electrostatic. The inductive electric field does, however, gives an important contribution to the parallel electric field. The electric and magnetic fields are most conveniently written in terms of the scalar potential ϕ and vector potential $\boldsymbol{A}$:

$$\delta\boldsymbol{E} = -\nabla\phi - \frac{1}{c}\frac{\partial\boldsymbol{A}}{\partial t}, \quad \delta\boldsymbol{B} = \nabla \times \boldsymbol{A}. \tag{A4}$$

We choose the Coulomb gauge $\nabla \cdot \boldsymbol{A} = 0$. Thus, with the gyrokinetic ordering, to $O(\epsilon^2)$, the vector potential is

$$\boldsymbol{A} = A_\parallel \hat{z} + \boldsymbol{A}_\perp = A_\parallel \hat{z} + \nabla\lambda \times \hat{z}. \tag{A5}$$

Hence, the perturbed magnetic field to $O(\epsilon^2)$ is given by

$$\delta\boldsymbol{B} = \nabla A_\parallel \times \hat{z} - \nabla^2\lambda\hat{z} = \nabla A_\parallel \times \hat{z} + \delta B_\parallel \hat{z}. \tag{A6}$$

We use the scalars $A_\parallel$ and $\delta B_\parallel$ (rather than λ) in subsequent development.

Consider next the Ampère-Maxwell law:

$$\nabla \times \delta\boldsymbol{B} = \frac{4\pi}{c}\delta\boldsymbol{j} + \frac{1}{c}\frac{\partial \delta\boldsymbol{E}}{\partial t}. \tag{A7}$$

The left-hand side is $O(\epsilon B_0 \Omega_i/v_{\mathrm{th}_i})$, while the second term in the left-hand side (the displacement current) is $O(\epsilon^2 B_0 \Omega_i v_{\mathrm{th}_i}/c^2)$. The ratio of the latter to the former is, therefore, $O(\epsilon v_{\mathrm{th}_i}^2/c^2)$, so we can drop the displacement current and use the pre-Maxwell form of Ampère's law:

$$\nabla \times \delta\boldsymbol{B} = -\nabla^2\boldsymbol{A} = -\nabla^2 A_\parallel \hat{z} + \nabla\delta B_\parallel \times \hat{z} = \frac{4\pi}{c}\delta\boldsymbol{j}. \tag{A8}$$

A2. THE GYROKINETIC EQUATION

Let us start with the Fokker-Planck equation

$$\frac{df_s}{dt} = \frac{\partial f_s}{\partial t} + \boldsymbol{v}\cdot\nabla f_s + \frac{q_s}{m_s}\left(-\nabla\phi - \frac{1}{c}\frac{\partial\boldsymbol{A}}{\partial t} + \frac{\boldsymbol{v}\times\boldsymbol{B}}{c}\right)\cdot\frac{\partial f_s}{\partial \boldsymbol{v}} = \left(\frac{\partial f_s}{\partial t}\right)_{\mathrm{coll}} = C_{sr}(f_s, f_r) + C_{ss}(f_s, f_s), \tag{A9}$$

where the right-hand side is the standard Fokker-Planck integrodifferential collision operator (e.g., Helander & Sigmar 2002). The expression $C_{sr}(f_s, f_r)$ denotes the effect of collisions of species s on (the other) species r, and $C_{ss}(f_s, f_s)$ denotes like-particle collisions. To reduce the clutter, we suppress the species label s in this section and denote the entire collision term by $C(f, f)$.

The distribution function is expanded in powers of ϵ:

$$f = F_0 + \delta f, \quad \delta f = \delta f_1 + \delta f_2 + \dots, \tag{A10}$$

where $\delta f_n \sim O(\epsilon^n F_0)$. With the ordering defined by equations (8)–(13), the terms in the Fokker-Planck are ordered as follows:

$$\begin{array}{cccc}
\dfrac{\partial F_0/\partial t}{\epsilon^2} & +\dfrac{\partial\delta f/\partial t}{\epsilon} & +\dfrac{\boldsymbol{v}_\perp\cdot\nabla\delta f}{1} & +\dfrac{v_\parallel\hat{z}\cdot\nabla\delta f}{\epsilon} \\[2ex]
+\dfrac{q}{mc}(-c\nabla\phi) & -\partial\boldsymbol{A}/\partial t & +\boldsymbol{v}\times\delta\boldsymbol{B} & +(\boldsymbol{v}\times\boldsymbol{B}_0)\cdot\partial F_0/\partial\boldsymbol{v} \\[0.5ex]
1 & \epsilon & 1 & 1/\epsilon \\[2ex]
+\dfrac{q}{mc}(-c\nabla\phi) & -\partial\boldsymbol{A}/\partial t & +\boldsymbol{v}\times\delta\boldsymbol{B} & +(\boldsymbol{v}\times\boldsymbol{B}_0)\cdot\partial\delta f/\partial\boldsymbol{v} \\[0.5ex]
\epsilon & \epsilon^2 & \epsilon & 1 \\[2ex]
=C(F_0, F_0) & +C(\delta f, F_0) & +C(F_0, \delta f) & +C(\delta f, \delta f), \\[0.5ex]
1 & \epsilon & \epsilon & \epsilon^2
\end{array} \tag{A11}$$

[11] Alternatively, one can say that the divergence of the electric field is small for gyrokinetic perturbations whose wavelengths are long compared to the electron Debye length, $\lambda_{\mathrm{D}e}$.

where we label below each term its order relative to $F_0 v_{\text{th}_i}/l_0$. We now proceed with the formal expansion.

A2.1. Minus First Order, $O(1/\epsilon)$

From equation (A11), in velocity variables transformed from $\boldsymbol{v}$ to $(v, v_\perp, \theta)$, we obtain at this order

$$\frac{\partial F_0}{\partial \theta} = 0, \tag{A12}$$

so the equilibrium distribution function does not depend on gyrophase angle, $F_0 = F_0(v, v_\perp, t)$.

A2.2. Zeroth Order, $O(1)$

At this order, equation (A11) becomes

$$\boldsymbol{v}_\perp \cdot \nabla \delta f_1 + \frac{q}{m}\left(-\nabla\phi + \frac{\boldsymbol{v} \times \delta \boldsymbol{B}}{c}\right) \cdot \frac{\partial F_0}{\partial \boldsymbol{v}} - \Omega \frac{\partial \delta f_1}{\partial \theta} = C(F_0, F_0). \tag{A13}$$

At this stage both F_0 and δf_1 are unknown. To eliminate δf_1 from this equation (and thereby isolate information about F_0), we multiply equation (A13) by $1 + \ln F_0$ and integrate over all space and all velocities, making use of equation (A12) and assuming that perturbed quantities spatially average to zero (this is exactly true in a periodic box). We find

$$\int d^3\boldsymbol{r} \int d^3\boldsymbol{v} \, (\ln F_0) C(F_0, F_0) = 0. \tag{A14}$$

It is known from the proof of Boltzmann's H-theorem that this uniquely constrains F_0 to be a Maxwellian:

$$F_0 = \frac{n_0}{\pi^{3/2} v_{\text{th}}^3} \exp\left(-\frac{v^2}{v_{\text{th}}^2}\right), \tag{A15}$$

where the mean plasma flow is assumed to be zero. The temperature $T_0(t) = (1/2)mv_{\text{th}}^2$ associated with this Maxwellian varies on the slow (heating) timescale, $t_{\text{heat}} \sim O(\epsilon^{-2} l_0/v_{\text{th}})$, due to conversion of the turbulent energy into heat. In Appendix B, we determine this heating in the second order of the gyrokinetic expansion. The density n_0 does not vary because the number of particles is conserved. In most other derivations of gyrokinetics, F_0 is not determined, although it is often assumed to be a Maxwellian.

Substituting the solution for F_0 (eq. [A15]) into equation (A13) and using $C(F_0, F_0) = 0$ yields

$$\boldsymbol{v}_\perp \cdot \nabla \delta f_1 - \Omega \frac{\partial \delta f_1}{\partial \theta} = -\boldsymbol{v} \cdot \nabla\left(\frac{q\phi}{T_0}\right) F_0. \tag{A16}$$

This inhomogeneous equation for δf_1 supports a particular solution and a homogeneous solution. Noting the particular solution $\delta f_p = -(q\phi/T_0)F_0 + O(\epsilon^2 F_0)$, the first-order perturbation is written as $\delta f_1 = -(q\phi/T_0)F_0 + h$, where the homogeneous solution h satisfies

$$\boldsymbol{v}_\perp \cdot \nabla h - \Omega\left(\frac{\partial h}{\partial \theta}\right)_{\boldsymbol{r}} = \left(\frac{\partial h}{\partial \theta}\right)_{\boldsymbol{R}} = 0, \tag{A17}$$

where we have transformed the θ derivative at constant position $\boldsymbol{r}$ to one at constant guiding center $\boldsymbol{R}$. Thus, h is independent of the gyrophase angle at constant guiding center $\boldsymbol{R}$ (but not at constant position $\boldsymbol{r}$): $h = h(\boldsymbol{R}, v, v_\perp, t)$. Therefore, the complete solution for the distribution function, after taking $1 - q\phi/T_0 = \exp(-q\phi/T_0) + O(\epsilon^2)$ and absorbing $O(\epsilon^2)$ terms into δf_2, is

$$f = F_0(v, \epsilon^2 t) \exp\left[-\frac{q\phi(\boldsymbol{r}, t)}{T_0}\right] + h(\boldsymbol{R}, v, v_\perp, t) + \delta f_2 + \dots \tag{A18}$$

The first term in the solution is the equilibrium distribution function corrected by the Boltzmann factor. Physically this arises from the rapid (compared to the evolution of ϕ) motion of electrons along and ions across the field lines attempting to set up a thermal equilibrium distribution. However, the motion of the particles across the field is constrained by the gyration, and the particles are not (entirely) free to set up thermal equilibrium. The second term is the gyrokinetic distribution function that represents the response of the rings to the perturbed fields.

A2.3. First Order, $O(\epsilon)$

Plugging in the form of solution given in equation (A18) and transforming into guiding-center spatial coordinates and velocity coordinates $(v, v_\perp, \theta)$, the Fokker-Planck equation to this order becomes

$$\frac{\partial h}{\partial t} + \frac{d\boldsymbol{R}}{dt} \cdot \frac{\partial h}{\partial \boldsymbol{R}} + \frac{q}{m}\left(-\nabla_\perp \phi + \frac{\boldsymbol{v} \times \delta \boldsymbol{B}}{c}\right) \cdot \left(\frac{\boldsymbol{v}}{v}\frac{\partial h}{\partial v} + \frac{\boldsymbol{v}_\perp}{v_\perp}\frac{\partial h}{\partial v_\perp}\right) - C(h, F_0) - C(F_0, h) = \Omega\left(\frac{\partial \delta f_2}{\partial \theta}\right)_{\boldsymbol{R}} + \frac{q}{T_0}\left(\frac{\partial \phi}{\partial t} - \frac{\boldsymbol{v}}{c} \cdot \frac{\partial \boldsymbol{A}}{\partial t}\right)F_0, \tag{A19}$$

where

$$\frac{d\mathbf{R}}{dt} = v_\parallel \hat{z} + \frac{c}{B_0}\left(-\nabla\phi - \frac{1}{c}\frac{\partial \mathbf{A}}{\partial t} + \frac{\mathbf{v}\times\delta\mathbf{B}}{c}\right)\times\hat{z}. \tag{A20}$$

Note that the linearized collision operator $C(h, F_0) + C(F_0, h)$ involves h and F_0 both of electrons and of ions.

To eliminate δf_2 from equation (A19), we ring average the equation over θ at fixed guiding center $\mathbf{R}$, taking advantage of the fact that δf_2 must be periodic in θ. The ring averaging also eliminates the third term on the left-hand side. Indeed, for an arbitrary function $a(\mathbf{r})$,

$$\langle \mathbf{v}_\perp\cdot\nabla a\rangle_{\mathbf{R}} = -\Omega\left\langle (\mathbf{v}\times\hat{z})\cdot\left(\frac{\partial}{\partial \mathbf{v}}\frac{\mathbf{v}\times\hat{z}}{\Omega}\right)\cdot\nabla a\right\rangle_{\mathbf{R}} = \Omega\left\langle (\mathbf{v}\times\hat{z})\cdot\left(\frac{\partial \mathbf{r}}{\partial \mathbf{v}}\right)_{\mathbf{R}}\cdot\nabla a\right\rangle_{\mathbf{R}} = \Omega\left\langle (\mathbf{v}\times\hat{z})\cdot\left(\frac{\partial a}{\partial \mathbf{v}}\right)_{\mathbf{R}}\right\rangle_{\mathbf{R}} = -\Omega\left\langle\left(\frac{\partial a}{\partial \theta}\right)_{\mathbf{R}}\right\rangle_{\mathbf{R}} = 0, \tag{A21}$$

from which $\langle \mathbf{v}\cdot\nabla_\perp\phi\rangle_{\mathbf{R}} = 0$ and $\langle \mathbf{v}_\perp\cdot(\mathbf{v}\times\delta\mathbf{B})\rangle_{\mathbf{R}} = v_\parallel\langle \mathbf{v}_\perp\cdot(\hat{z}\times\delta\mathbf{B})\rangle_{\mathbf{R}} = v_\parallel\langle \mathbf{v}_\perp\cdot\nabla_\perp A_\parallel\rangle_{\mathbf{R}} = 0$ (see eq. [A6]). Thus, the ring-averaged equation (A19) takes the form

$$\frac{\partial h}{\partial t} + \left\langle\frac{d\mathbf{R}}{dt}\right\rangle_{\mathbf{R}}\cdot\frac{\partial h}{\partial \mathbf{R}} - \left(\frac{\partial h}{\partial t}\right)_{\mathrm{coll}} = \frac{q}{T_0}\frac{\partial\langle\chi\rangle_{\mathbf{R}}}{\partial t}F_0, \tag{A22}$$

where we have defined the gyrokinetic collision operator $(\partial h/\partial t)_{\mathrm{coll}} = \langle C(h, F_0) + C(F_0, h)\rangle_{\mathbf{R}}$ and the gyrokinetic potential $\chi = \phi - \mathbf{v}\cdot\mathbf{A}/c$. Keeping only first-order contributions in equation (A20) and substituting for $\delta\mathbf{B}$ from equation (A6), we find that the ring-averaged guiding center motion is given by

$$\left\langle\frac{d\mathbf{R}}{dt}\right\rangle_{\mathbf{R}} = v_\parallel\hat{z} - \frac{c}{B_0}\langle\nabla_\perp\phi\rangle_{\mathbf{R}}\times\hat{z} + \frac{v_\parallel}{B_0}\langle\nabla_\perp A_\parallel\rangle_{\mathbf{R}}\times\hat{z} - \frac{1}{B_0}\langle \mathbf{v}_\perp\delta B_\parallel\rangle_{\mathbf{R}} = v_\parallel\hat{z} - \frac{c}{B_0}\frac{\partial\langle\chi\rangle_{\mathbf{R}}}{\partial \mathbf{R}}\times\hat{z}, \tag{A23}$$

where we have used the identity $\langle \mathbf{v}_\perp\delta B_\parallel\rangle_{\mathbf{R}} = -\langle\nabla_\perp(\mathbf{v}_\perp\cdot\mathbf{A}_\perp)\rangle_{\mathbf{R}}$. Substituting equation (A23) into equation (A22), we obtain the *gyrokinetic equation*:

$$\frac{\partial h}{\partial t} + v_\parallel\hat{z}\cdot\frac{\partial h}{\partial \mathbf{R}} + \frac{c}{B_0}[\langle\chi\rangle_{\mathbf{R}}, h] - \left(\frac{\partial h}{\partial t}\right)_{\mathrm{coll}} = \frac{q}{T_0}\frac{\partial\langle\chi\rangle_{\mathbf{R}}}{\partial t}F_0, \tag{A24}$$

where the nonlinear effects enter via the Poisson bracket, defined by

$$[\langle\chi\rangle_{\mathbf{R}}, h] = \left(\frac{\partial\langle\chi\rangle_{\mathbf{R}}}{\partial \mathbf{R}}\times\hat{z}\right)\cdot\frac{\partial h}{\partial \mathbf{R}} = \frac{\partial\langle\chi\rangle_{\mathbf{R}}}{\partial X}\frac{\partial h}{\partial Y} - \frac{\partial\langle\chi\rangle_{\mathbf{R}}}{\partial Y}\frac{\partial h}{\partial X}. \tag{A25}$$

The gyrokinetic equation (A24) describes the time evolution of h, the ring distribution function. The second term on the left-hand side corresponds to the ring motion along $\mathbf{B}_0$, the third term to the ring motion across $\mathbf{B}_0$, and the fourth term to the effect of collisions. The source term on the right-hand side is the ring-averaged change in the energy of the particles. A more detailed discussion of the physical aspects of this equation is given in § 2.4. The equilibrium distribution function F_0 changes only on the slow (heating) timescale and is thus formally fixed (stationary) with respect to the timescale of equation (A24). The evolution of F_0 is calculated in Appendix B.

A3. THE GYROKINETIC FORM OF MAXWELL'S EQUATIONS

To complete the set of gyrokinetic equations, we need to determine the electromagnetic field, which is encoded by χ. To determine the three unknown scalars ϕ, $A_\parallel$, and $\delta B_\parallel$ (which relates to $\mathbf{A}_\perp$ via eqs. [A4] and [A6]), we use the quasineutrality condition, equation (A2), and Ampère's law, equation (A8), taken at $O(\epsilon)$ in the gyrokinetic ordering.

A3.1. The Quasineutrality Condition

The charge density needed in the quasineutrality condition, equation (A2), can be determined by multiplying the distribution function, equation (A18), expanded to first order $O(\epsilon)$, by the charge q_s and integrating over velocities. Expanding the exponential in the Boltzmann term and dropping terms of order $O(\epsilon^2)$ and higher gives

$$\sum_s\left[-\frac{q_s^2 n_{0s}}{T_{0s}}\phi + q_s\int d^3\mathbf{v}\, h_s\left(\mathbf{r} + \frac{\mathbf{v}\times\hat{z}}{\Omega_s}, \mathbf{v}, t\right)\right] = 0. \tag{A26}$$

Note that the velocity integral must be performed at a fixed position $\mathbf{r}$, because the charge must be determined at a fixed position $\mathbf{r}$, not at a fixed guiding center $\mathbf{R}$. Using the ring average at constant $\mathbf{r}$ (eq. [22]), the quasineutrality condition can be written in the following form

$$\sum_s\left(-\frac{q_s^2 n_{0s}}{T_{0s}}\phi + q_s\int d^3\mathbf{v}\,\langle h_s\rangle_{\mathbf{r}}\right) = 0. \tag{A27}$$

A3.2. The Parallel Ampère's Law

The current density is calculated by multiplying the distribution function, equation (A18), expanded to first order $O(\epsilon)$, by $q_s \boldsymbol{v}$ and integrating over velocities. The Boltzmann part of the current is odd with respect to $v_\parallel$ and vanishes on integration. The parallel component of Ampère's law, equation (A8), is, therefore,

$$-\nabla_\perp^2 A_\parallel = \frac{4\pi}{c}\delta j_\parallel = \sum_s \frac{4\pi}{c} q_s \int d^3\boldsymbol{v}\, v_\parallel \langle h_s \rangle_{\boldsymbol{r}}, \tag{A28}$$

where the ring average at a fixed position $\boldsymbol{r}$ appears in the same fashion as in equation (A27).

A3.3. The Perpendicular Ampère's Law

The perpendicular component of Ampère's law, equation (A8), is derived in an analogous manner as the parallel component in Appendix A.3.2: Ampère's law is crossed with $\hat{z}$, the Boltzmann contribution vanishes on integration over gyrophase angle θ, and a ring average at a fixed position $\boldsymbol{r}$ is performed. The result is

$$\nabla_\perp \delta B_\parallel = \frac{4\pi}{c}\hat{z} \times \delta\boldsymbol{j} = \sum_s \frac{4\pi}{c} q_s \int d^3\boldsymbol{v}\, \langle \hat{z} \times \boldsymbol{v}_\perp h_s \rangle_{\boldsymbol{r}}. \tag{A29}$$

It is straightforward to show that equation (A29) is the gyrokinetic version of perpendicular pressure balance (no fast magnetosonic waves). Integration by parts yields

$$\nabla_\perp \frac{B_0 \delta B_\parallel}{4\pi} = -\nabla_\perp \cdot \delta\boldsymbol{P}_\perp, \tag{A30}$$

where the perpendicular pressure tensor is

$$\delta\boldsymbol{P}_\perp = \sum_s m_s \int d^3\boldsymbol{v}\, \langle \boldsymbol{v}_\perp \boldsymbol{v}_\perp h_s \rangle_{\boldsymbol{r}}. \tag{A31}$$

In order to drive steady state (nondecaying) turbulence, we introduce an additional externally driven antenna current $\boldsymbol{j}_a$ to the right-hand sides of equations (A28) and (A29).

APPENDIX B

DERIVATION OF THE HEATING EQUATION

While the gyrokinetic equation (A24) determines the evolution of the perturbation to the distribution function on the intermediate timescale, we must go to second order, $O(\epsilon^2\omega)$, in the gyrokinetic ordering to obtain the slow evolution of the equilibrium distribution function F_0. This appendix contains two derivations of the heating equation (39): the first is more conventional, but longer (Appendix B.1); the second employs entropy conservation and is, in a sense, more intuitive and fundamental (Appendix B.2). We also discuss energy conservation in driven systems and derive the power balance equation (40) (see Appendix B.3).

B1. CONVENTIONAL DERIVATION OF THE HEATING EQUATION

We begin by defining the medium-time average over a period Δt long compared to the fluctuation timescale but short compared to the heating timescale, $1/\omega \ll \Delta t \ll 1/\epsilon^2\omega$,

$$\overline{a}(t) = \frac{1}{\Delta t} \int_{t-\Delta t/2}^{t+\Delta t/2} dt'\, a(t'). \tag{B1}$$

The equilibrium distribution function F_0 is constant at times $\sim \Delta t$, so $\overline{F_0} = F_0$.

To determine the evolution of the equilibrium density and temperature of a species s on the heating (transport) timescale, we consider the full (not ring-averaged) Fokker-Planck equation (A9). To demonstrate that particle conservation implies that n_{0s} is a constant, we integrate equation (A9) over *all* space and velocity, divide by system volume V, and discard all terms of order $O(\epsilon^3)$ and higher:

$$\int \frac{d^3\boldsymbol{r}}{V} \int d^3\boldsymbol{v}\, \frac{\partial f_s}{\partial t} = \frac{dn_{0s}}{dt} + \frac{d}{dt}\int \frac{d^3\boldsymbol{r}}{V} \int d^3\boldsymbol{v}\, \delta f_{2s} = 0. \tag{B2}$$

Here we have used the conservation of particles by the collision operator, the fact that the first-order perturbations spatially average to zero, and an integration by parts over velocity to simplify the result. Performing the medium-time average (eq. [B1]) eliminates the δf_{2s} term, leaving

$$\frac{dn_{0s}}{dt} = 0. \tag{B3}$$

Thus, for both species s, the density n_{0s} is constant on the heating (transport) timescale.

The evolution of the temperature T_{0s} is calculated similarly by multiplying equation (A9) by $m_s v^2/2$, integrating over all space and velocity, and dividing by the system volume V. Using the expansion of the distribution function, integration by parts in velocity, we get

$$\frac{3}{2} n_{0s} \frac{dT_{0s}}{dt} + \frac{d}{dt} \int \frac{d^3 \boldsymbol{r}}{V} \int d^3 \boldsymbol{v} \frac{m_s v^2}{2} \delta f_{2s} = \int \frac{d^3 \boldsymbol{r}}{V} \int d^3 \boldsymbol{v} \, q_s (\boldsymbol{v} \cdot \boldsymbol{E}) f_s + \int \frac{d^3 \boldsymbol{r}}{V} \int d^3 \boldsymbol{v} \frac{m_s v^2}{2} C_{sr}(f_s, f_r). \tag{B4}$$

We have again assumed $\int d^3 \boldsymbol{r} \, \delta f_{1s} = 0$ (first-order perturbations spatially average to zero). The first term on the right-hand side is the work done on the particles by the fields, and the second is the collisional energy exchange between species. Note that collisions between like particles do not produce a net loss of energy for a species and thus do not appear in this expression (the operator C_{ss} integrates to zero). At this order, the collisions between species occur only between the Maxwellian equilibria of each interacting species; the standard form of this collisional energy exchange (see, e.g., Helander & Sigmar 2002) is given by

$$\int \frac{d^3 \boldsymbol{r}}{V} \int d^3 \boldsymbol{v} \frac{m_s v^2}{2} C_{sr}(f_s, f_r) = n_{0s} \nu_E^{sr} (T_{0r} - T_{0s}). \tag{B5}$$

Expressions for the interspecies collision rate ν_E^{sr} can be found in Helander & Sigmar (2002). The collisional energy exchange rate of ions on electrons, ν_E^{ie}, is a factor $(m_e/m_i)^{1/2}$ times smaller than the ion-ion collision rate. It is, therefore, possible to sustain a temperature difference between ions and electrons even though the plasma is collisional enough to make F_0 Maxwellian for each species.

Splitting the electric field into potentials, $\boldsymbol{E} = -\nabla \phi - (1/c)\partial \boldsymbol{A}/\partial t$, we can manipulate the scalar potential part into a more useful higher order form. After some algebra and using equation (B5), we find

$$\frac{3}{2} n_{0s} \frac{dT_{0s}}{dt} + \frac{d}{dt} \int \frac{d^3 \boldsymbol{r}}{V} \int d^3 \boldsymbol{v} \left(\frac{m_s v^2}{2} \delta f_{2s} + q_s \phi \delta f_s \right) = \int \frac{d^3 \boldsymbol{r}}{V} \int d^3 \boldsymbol{v} \, q_s \frac{\partial}{\partial t} \left(\phi - \frac{\boldsymbol{v} \cdot \boldsymbol{A}}{c} \right) \delta f_s + n_{0s} \nu_E^{sr} (T_{0r} - T_{0s}), \tag{B6}$$

where δf_s is the entire perturbed part of the distribution function. From this equation, we can check the order of the heating rate,

$$\frac{3}{2} n_{0s} \frac{dT_{0s}}{dt} \sim O(\epsilon^2 \omega T_{0s}). \tag{B7}$$

We see that the variation in the equilibrium quantities is, as expected, on a timescale that is ϵ^2 slower than the timescale of the variations in the fluctuating quantities. Note that this ordering is consistent with all the energy in an Alfvén wave cascade becoming heat in a single cascade time at the driving scale.

Splitting the perturbed distribution function δf_s into the Boltzmann and gyrokinetic parts (eq. [A18]), we obtain the following instantaneous form of the *heating equation*

$$\frac{3}{2} n_{0s} \frac{dT_{0s}}{dt} + \frac{d}{dt} \left[\int \frac{d^3 \boldsymbol{r}}{V} \int d^3 \boldsymbol{v} \left(\frac{m_s v^2}{2} \delta f_{2s} + q_s \phi h_s \right) - \int \frac{d^3 \boldsymbol{r}}{V} \frac{n_{0s} q_s^2 \phi^2}{2 T_{0s}} \right] = \int \frac{d^3 \boldsymbol{r}}{V} \int d^3 \boldsymbol{v} \, q_s \frac{\partial \chi}{\partial t} h_s + n_{0s} \nu_E^{sr} (T_{0r} - T_{0s}). \tag{B8}$$

To obtain the heating equation (39), we take the medium-time average, defined by equation (B1), of the above equation. The average of the second term on the left-hand side is zero; it does not contribute to the average heating. Thus, we do not require the second-order perturbed distribution function δf_{2s} to calculate the heating. The average of the first term on the right-hand side of equation (B8) is the desired heating term that relates the slow-timescale evolution of the equilibrium to the solution of the gyrokinetic equation. The $\boldsymbol{r}$ integral is converted into the $\boldsymbol{R}_s$ integral by noticing that $\int d^3 \boldsymbol{r} \int d^3 \boldsymbol{v} = \int d^3 \boldsymbol{v} \int d^3 \boldsymbol{R}_s$ (the velocity integration on the left is at constant $\boldsymbol{r}$, while on the right it is at constant $\boldsymbol{R}_s$). Therefore,

$$\int \frac{d^3 \boldsymbol{r}}{V} \int d^3 \boldsymbol{v} \, q_s \frac{\partial \chi(\boldsymbol{r})}{\partial t} h_s(\boldsymbol{R}_s) = \int d^3 \boldsymbol{v} \int \frac{d^3 \boldsymbol{R}_s}{V} q_s \left[\frac{\partial}{\partial t} \chi \left(\boldsymbol{R}_s - \frac{\boldsymbol{v} \times \hat{\boldsymbol{z}}}{\Omega_s} \right) \right] h_s(\boldsymbol{R}_s) = \int d^3 \boldsymbol{v} \int \frac{d^3 \boldsymbol{R}_s}{V} q_s \frac{\partial \langle \chi \rangle_{\boldsymbol{R}_s}}{\partial t} h_s. \tag{B9}$$

We must now demonstrate that the heating is ultimately collisional (the second equality in eq. [39]). To make this connection, we multiply the gyrokinetic equation (A24) by $T_{0s} h_s/F_{0s}$ and integrate over space (i.e., with respect to $\boldsymbol{R}_s$) and velocity to obtain the following equation

$$\frac{d}{dt} \int d^3 \boldsymbol{v} \int \frac{d^3 \boldsymbol{R}_s}{V} \frac{T_{0s}}{2 F_{0s}} h_s^2 - \int d^3 \boldsymbol{v} \int \frac{d^3 \boldsymbol{R}_s}{V} \frac{T_{0s}}{F_{0s}} h_s \left(\frac{\partial h_s}{\partial t} \right)_{\text{coll}} = \int d^3 \boldsymbol{v} \int \frac{d^3 \boldsymbol{R}_s}{V} q_s \frac{\partial \langle \chi \rangle_{\boldsymbol{R}_s}}{\partial t} h_s \tag{B10}$$

(for reasons that become apparent in Appendix B.2, this is referred to as the *entropy-balance equation*). Combining equations (B8) and (B10) using equation (B9) then gives the collisional form of the instantaneous heating equation:

$$\frac{3}{2} n_{0s} \frac{dT_{0s}}{dt} + \frac{d}{dt} \left[\int \frac{d^3 \boldsymbol{r}}{V} \int d^3 \boldsymbol{v} \left(\frac{m_s v^2}{2} \delta f_{2s} + q_s \phi \langle h_s \rangle_{\boldsymbol{r}} - \frac{T_{0s}}{2 F_{0s}} \langle h_s^2 \rangle_{\boldsymbol{r}} \right) - \int \frac{d^3 \boldsymbol{r}}{V} \frac{n_{0s} q_s^2 \phi^2}{2 T_{0s}} \right]$$
$$= - \int \frac{d^3 \boldsymbol{r}}{V} \int d^3 \boldsymbol{v} \frac{T_{0s}}{F_{0s}} \left\langle h_s \left(\frac{\partial h_s}{\partial t} \right)_{\text{coll}} \right\rangle_{\boldsymbol{r}} + n_{0s} \nu_E^{sr} (T_{0r} - T_{0s}), \tag{B11}$$

where we have used $\int d^3\boldsymbol{r} \int d^3\boldsymbol{v}\, a(\boldsymbol{R}_s) = \int d^3\boldsymbol{r} \int d^3\boldsymbol{v}\, \langle a \rangle_{\boldsymbol{r}}$ (this manipulation is done purely for notational cleanliness: the expressions under the integrals are now explicitly functions of $\boldsymbol{r}$ and $\boldsymbol{v}$, not of $\boldsymbol{R}_s$). Under medium-time averaging, the second term on the left-hand side of equation (B11) again vanishes, and the second equality in equation (39) is obtained:

$$\frac{3}{2} n_{0s} \frac{dT_{0s}}{dt} = -\int \frac{d^3\boldsymbol{r}}{V} \int d^3\boldsymbol{v}\, \frac{T_{0s}}{F_{0s}} \overline{\left\langle h_s \left(\frac{\partial h_s}{\partial t} \right)_{\mathrm{coll}} \right\rangle_{\boldsymbol{r}}} + n_{0s} \nu_E^{sr}(T_{0r} - T_{0s}).$$ (B12)

The term that has averaged out does not contribute to the net (slow-timescale) heating because it represents the sloshing of energy back and forth between particles and fields (on the fluctuation timescale). On the right-hand side, the collisional term is negative definite for like-particle and pitch-angle collision operators. [These are the only relevant cases: for $s = i$, the ion-ion collisions dominate, and for $s = e$, the dominant terms are electron-electron collisions and the pitch-angle scattering of the electrons off the ions; all other parts of the collision operator are subdominant by at least one factor of $(m_e/m_i)^{1/2}$.]

The equation (B12) for the heating on the slow timescale is sign-definite, so it is, in practice, easier to average numerically than the instantaneous heating equation (B8): unlike in equation (B8), calculating the average heating does not require precisely capturing the effect of near-cancellation of the intermediate-timescale oscillations of the instantaneous energy transfer between particles and waves. The net heating is always collisional, regardless of the collision rate—when collisions are small, h_s develops small scales in velocity space, typically $\Delta \boldsymbol{v} \sim O(\nu^{1/2})$, so that the heating is independent of the collision rate ν. As we shall see below, equation (B12) relates heating to the collisional entropy production.

B2. ENTROPY ARGUMENT TO DERIVE THE HEATING EQUATION

Ignoring the ion-electron collisions, whose rate is $(m_e/m_i)^{1/2}$ times smaller than that of the ion-ion collisions, Boltzmann's H-theorem gives the time evolution of the entropy of the ions S_i as follows:

$$\frac{dS_i}{dt} = -\frac{d}{dt} \int \frac{d^3\boldsymbol{r}}{V} \int d^3\boldsymbol{v}\, f_i \ln f_i = -\int \frac{d^3\boldsymbol{r}}{V} \int d^3\boldsymbol{v}\, \ln f_i\, C_{ii}(f_i, f_i).$$ (B13)

It can be easily shown that the right-hand side is nonnegative (see, e.g., Lifshitz & Pitaevskii 1981) and, therefore, that entropy always increases. It can also be shown that the entropy increase is zero if, and only if, the distribution function is a Maxwellian. Expanding f_i about the Maxwellian F_{0i}, we obtain, to order $O(\epsilon^2)$,

$$\frac{dS_i}{dt} = -\frac{d}{dt} \int \frac{d^3\boldsymbol{r}}{V} \int d^3\boldsymbol{v} \left[F_{0i} \ln F_{0i} + (1 + \ln F_{0i})\delta f_{2i} + \frac{\delta f_{1i}^2}{2F_{0i}} \right] = -\int \frac{d^3\boldsymbol{r}}{V} \int d^3\boldsymbol{v}\, \frac{\delta f_{1i}}{F_{0i}} \left(\frac{\partial \delta f_{1i}}{\partial t} \right)_{\mathrm{coll}},$$ (B14)

where we have made use of the energy conservation properties of ion-ion collisions and of the fact that δf_{1i} spatially averages to zero. Evaluating the zeroth-order (Maxwellian) part of the integral on the left-hand side and splitting δf_{1i} into the Boltzmann and gyrokinetic parts (eq. [A18]), we obtain the slow evolution of temperature

$$\frac{3}{2} n_{0i} \frac{1}{T_{0i}} \frac{dT_{0i}}{dt} + \frac{d}{dt} \left[\int \frac{d^3\boldsymbol{r}}{V} \int d^3\boldsymbol{v} \left(\frac{m_i v^2}{2T_{0i}} \delta f_{2i} + \frac{q_i\phi}{T_{0i}} h_i - \frac{h_i^2}{2F_{0i}} \right) - \int \frac{d^3\boldsymbol{r}}{V} \frac{n_{0i} q_i^2 \phi^2}{2T_{0i}^2} \right] = -\int \frac{d^3\boldsymbol{r}}{V} \int d^3\boldsymbol{v}\, \frac{1}{F_{0i}} \left\langle h_i \left(\frac{\partial h_i}{\partial t} \right)_{\mathrm{coll}} \right\rangle_{\boldsymbol{r}}.$$ (B15)

This result is the same as equation (B11); the heating is now manifestly expressed as the irreversible entropy production. Under medium-time average, the second term on the left-hand side of equation again vanishes, so the heating equation (B12) is recovered.

B3. ENERGY CONSERVATION IN DRIVEN SYSTEMS

To determine an equation for the conservation of energy in gyrokinetics, we use Poynting's theorem

$$\frac{d}{dt} \int d^3\boldsymbol{r} \left(\frac{E^2}{8\pi} + \frac{B^2}{8\pi} \right) + \frac{c}{4\pi} \oint d\boldsymbol{S} \cdot (\boldsymbol{E} \times \boldsymbol{B}) = -\int d^3\boldsymbol{r}\, (\boldsymbol{j} + \boldsymbol{j}_a) \cdot \boldsymbol{E},$$ (B16)

where $\boldsymbol{j}_a$ is the current in the antenna driving the system and $\boldsymbol{j}$ is the plasma current. We shall drop the surface term (the Poynting flux)—this is justified, e.g., in a numerical box with periodic boundary conditions.

From § 2.1, we know that $|\delta \boldsymbol{E}|^2 \sim O(\epsilon^2 B_0^2 v_{\mathrm{th}}^2/c^2)$ and $|\delta \boldsymbol{B}|^2 \sim O(\epsilon^2 B_0^2)$ (eq. [8]). Thus, in the nonrelativistic limit, the magnetic energy dominates, and we may neglect the electric field energy (this is consistent with neglecting the displacement current in the nonrelativistic ordering). We are left with

$$\frac{d}{dt} \int d^3\boldsymbol{r}\, \frac{|\delta \boldsymbol{B}|^2}{8\pi} = -\int d^3\boldsymbol{r}\, (\boldsymbol{j} + \boldsymbol{j}_a) \cdot \boldsymbol{E}.$$ (B17)

Under medium-time averaging, the left-hand side vanishes, and we are left with the steady state balance:

$$\int d^3\boldsymbol{r}\, \overline{(\boldsymbol{j} + \boldsymbol{j}_a) \cdot \boldsymbol{E}} = 0.$$ (B18)

On the other hand, using equations (B4) and (B11) to calculate $\int d^3\boldsymbol{r}\,(\boldsymbol{j}\cdot\boldsymbol{E}) = \int d^3\boldsymbol{r}\sum_s\int d^3\boldsymbol{v}\,q_s(\boldsymbol{v}\cdot\boldsymbol{E})f_s$, we can convert equation (B17) into the following instantaneous *power-balance equation*

$$\frac{d}{dt}\int\frac{d^3\boldsymbol{r}}{V}\left[\sum_s\int d^3\boldsymbol{v}\,\frac{T_{0s}}{2F_{0s}}\left(h_s - \frac{q_s\phi}{T_{0s}}F_{0s}\right)^2 + \frac{|\delta\boldsymbol{B}|^2}{8\pi}\right] = \sum_s\int\frac{d^3\boldsymbol{r}}{V}\int d^3\boldsymbol{v}\,\frac{T_{0s}}{F_{0s}}\left\langle h_s\left(\frac{\partial h_s}{\partial t}\right)_{\mathrm{coll}}\right\rangle_{\boldsymbol{r}} - \int\frac{d^3\boldsymbol{r}}{V}\boldsymbol{j}_a\cdot\boldsymbol{E}. \quad (B19)$$

The first term on the right-hand side is the nonnegative-definite collisional entropy production (see eq. [B15]); the second term is the external energy input. The left-hand side is the time derivative of the fluctuation energy (kinetic plus magnetic):

$$\delta W = \int\frac{d^3\boldsymbol{r}}{V}\left[\sum_s\int d^3\boldsymbol{v}\,\frac{T_{0s}\delta f_s^2}{2F_{0s}} + \frac{|\delta\boldsymbol{B}|^2}{8\pi}\right]. \quad (B20)$$

Note that in the large-scale limit, appropriate for MHD, we have Alfvén waves, for which $h_s\simeq q_s\langle\phi\rangle_{\boldsymbol{R}_s}/T_{0s}$—the kinetic energy then becomes the $\boldsymbol{E}\times\boldsymbol{B}$ velocity squared as it should be in MHD.

If we medium-time average equation (B19), the left-hand side vanishes, and we have the power balance between external energy injection and collisional dissipation:

$$\sum_s\int\frac{d^3\boldsymbol{r}}{V}\int d^3\boldsymbol{v}\,\frac{T_{0s}}{F_{0s}}\overline{\left\langle h_s\left(\frac{\partial h_s}{\partial t}\right)_{\mathrm{coll}}\right\rangle_{\boldsymbol{r}}} = \int\frac{d^3\boldsymbol{r}}{V}\overline{\boldsymbol{j}_a\cdot\boldsymbol{E}}. \quad (B21)$$

APPENDIX C

DERIVATION OF THE LINEAR COLLISIONLESS DISPERSION RELATION

The dispersion relation for a linear, collisionless gyrokinetic system is derived beginning with the linearized collisionless version of the gyrokinetic equation (25),

$$\frac{\partial h_s}{\partial t} + v_\parallel\frac{\partial h_s}{\partial z} = \frac{q_s}{T_{0s}}F_{0s}\frac{\partial\langle\chi\rangle_{\boldsymbol{R}_s}}{\partial t}, \quad (C1)$$

and the field equations (A27)–(A29). First, the electromagnetic fields and the gyrokinetic distribution function are expanded in plane waves, allowing the ring averages appearing in the equations to be written as multiplications by Bessel functions. The gyrokinetic equation is then solved algebraically for the distribution function. Next, this solution is substituted into equations (A27)–(A29), and the integration over velocity is performed using the plasma dispersion function to simplify the parallel velocity integrals and modified Bessel functions to express the perpendicular velocity integrals. The condition for the existence of a solution to the resulting set of algebraic equations is the dispersion relation. In this appendix, the plasma species subscript s is suppressed when unnecessary.

C1. SOLVING FOR THE DISTRIBUTION FUNCTION

First, we decompose the electromagnetic potentials into plane wave solutions of the form $a(\boldsymbol{r}, t) = \hat{a}\exp\left[i(\boldsymbol{k}\cdot\boldsymbol{r} - \omega t)\right]$ (where a denotes χ, ϕ, or $\boldsymbol{A}$) and the gyrokinetic distribution function into solutions of the form $h(\boldsymbol{R}, v, v_\perp, t) = \hat{h}\exp\left[i(\boldsymbol{k}\cdot\boldsymbol{R} - \omega t)\right]$. To solve equation (C1) for $\hat{h}$, we need to express $\langle\chi\rangle_{\boldsymbol{R}}$ in algebraic terms. Under the plane wave decomposition, ring averages reduce to multiplications by Bessel functions. For example, the terms with the scalar potential ϕ in the definition of $\chi = \phi - \boldsymbol{v}\cdot\boldsymbol{A}/c$ yield

$$\langle\phi(\boldsymbol{r}, t)\rangle_{\boldsymbol{R}} = \hat{\phi}e^{i(\boldsymbol{k}\cdot\boldsymbol{R} - \omega t)}\frac{1}{2\pi}\oint d\theta\,\exp\left(i\frac{k_\perp v_\perp}{\Omega}\cos\theta\right) = J_0\left(\frac{k_\perp v_\perp}{\Omega}\right)\hat{\phi}e^{i(\boldsymbol{k}\cdot\boldsymbol{R} - \omega t)}. \quad (C2)$$

Here we have used the definition of the zeroth-order Bessel function (Abramowitz & Stegun 1972) and the relation between the position and guiding center, equation (19), noting that $\boldsymbol{k}\cdot(\hat{\boldsymbol{z}}\times\boldsymbol{v}/\Omega) = (k_\perp v_\perp/\Omega)\cos\theta$, where θ is the angle between $\boldsymbol{k}_\perp$ and the particle's instantaneous Larmor radius $\hat{\boldsymbol{z}}\times\boldsymbol{v}/\Omega$. After further algebraic manipulations of this kind, the ring-averaged potential $\langle\chi\rangle_{\boldsymbol{R}}$ can be written in terms of zeroth- and first-order Bessel functions,

$$\langle\chi\rangle_{\boldsymbol{R}} = \left[J_0\left(\frac{k_\perp v_\perp}{\Omega}\right)\left(\hat{\phi} - \frac{v_\parallel\hat{A}_\parallel}{c}\right) + \frac{J_1(k_\perp v_\perp/\Omega)}{k_\perp v_\perp/\Omega}\frac{mv_\perp^2}{q}\frac{\delta\hat{B}_\parallel}{B_0}\right]e^{i(\boldsymbol{k}\cdot\boldsymbol{R} - \omega t)}, \quad (C3)$$

where we have used the definition $\delta\hat{B}_\parallel = i(\boldsymbol{k}_\perp\times\hat{\boldsymbol{A}}_\perp)\cdot\hat{\boldsymbol{z}}$. Similarly, the ring average of the distribution function at constant $\boldsymbol{r}$ becomes

$$\langle h(\boldsymbol{R}, v, v_\perp, t)\rangle_{\boldsymbol{r}} = J_0\left(\frac{k_\perp v_\perp}{\Omega}\right)\hat{h}e^{i(\boldsymbol{k}\cdot\boldsymbol{r} - \omega t)}. \quad (C4)$$

The linearized gyrokinetic equation can now be solved for the distribution function:

$$\hat{h} = \frac{qF_0}{T_0}\frac{\omega}{\omega - k_\parallel v_\parallel}\langle\hat{\chi}\rangle_R. \tag{C5}$$

Using equation (C3), this can be written in terms of the potentials as follows:

$$\hat{h} = \frac{qF_0}{T_0}\left\{J_0\left(\frac{k_\perp v_\perp}{\Omega}\right)\frac{\omega\hat{A}_\parallel}{k_\parallel c} + \frac{\omega}{\omega - k_\parallel v_\parallel}\left[J_0\left(\frac{k_\perp v_\perp}{\Omega}\right)\left(\hat{\phi} - \frac{\omega\hat{A}_\parallel}{k_\parallel c}\right) + \frac{J_1(k_\perp v_\perp/\Omega)}{k_\perp v_\perp/\Omega}\frac{2v_\perp^2}{v_{th}^2}\frac{T_0}{q}\frac{\delta\hat{B}_\parallel}{B_0}\right]\right\}. \tag{C6}$$

C2. PERFORMING THE INTEGRATION OVER VELOCITY

Because the solution for the distribution function, equation (C6), is a product of functions of $v_\parallel$ and $v_\perp$, the integrals over velocity space, $\int d^3v = \int_{-\infty}^{\infty} dv_\parallel \int_0^\infty v_\perp \, dv_\perp \int_0^{2\pi} d\theta$, in equations (A27)–(A29) can be expressed in terms of plasma dispersion functions and modified Bessel functions.

Integrals over $v_\parallel$, when not immediately completed, are written in terms of the plasma dispersion function (Fried & Conte 1961)

$$Z(\xi) = \frac{1}{\sqrt{\pi}}\int_L dx \, \frac{e^{-x^2}}{x - \xi}, \tag{C7}$$

where $\xi = \omega/|k_\parallel|v_{th}$ and the integral is performed over the Landau contour from $-\infty$ to $+\infty$ below the pole at $x = \xi$ in the complex plane. Using this definition, we can write

$$\frac{1}{\sqrt{\pi}}\int \frac{dv_\parallel}{v_{th}} e^{-v_\parallel^2/v_{th}^2}\frac{\omega}{\omega - k_\parallel v_\parallel} = -\xi Z(\xi). \tag{C8}$$

Integrations over $v_\perp$ can be written in terms of modified Bessel functions. Three such integrals arise:

$$\Gamma_0(\alpha) = \int_0^\infty \frac{2v_\perp \, dv_\perp}{v_{th}^2}\left[J_0\left(\frac{k_\perp v_\perp}{\Omega}\right)\right]^2 e^{-v_\perp^2/v_{th}^2} = I_0(\alpha)e^{-\alpha},$$

$$\Gamma_1(\alpha) = \int_0^\infty \frac{2v_\perp \, dv_\perp}{v_{th}^2}\frac{2v_\perp^2}{v_{th}^2}\frac{J_0(k_\perp v_\perp/\Omega)J_1(k_\perp v_\perp/\Omega)}{k_\perp v_\perp/\Omega} e^{-v_\perp^2/v_{th}^2} = [I_0(\alpha) - I_1(\alpha)]e^{-\alpha},$$

$$\Gamma_2(\alpha) = \int_0^\infty \frac{2v_\perp \, dv_\perp}{v_{th}^2}\frac{4v_\perp^4}{v_{th}^4}\left[\frac{J_1(k_\perp v_\perp/\Omega)}{k_\perp v_\perp/\Omega}\right]^2 e^{-v_\perp^2/v_{th}^2} = 2\Gamma_1(\alpha), \tag{C9}$$

where I_0 and I_1 are the modified Bessel functions, $\alpha = k_\perp^2\rho^2/2$, and we have used the relation (Watson 1966),

$$\int_0^\infty dx\, xJ_n(px)J_n(qx)e^{-a^2x^2} = \frac{1}{2a^2}I_n\left(\frac{pq}{2a^2}\right)e^{-(p^2+q^2)/4a^2}. \tag{C10}$$

C3. QUASINEUTRALITY CONDITION

Beginning with the gyrokinetic quasineutrality condition, equation (A27), we write the ring average of the distribution function at constant position r as a multiplication by a Bessel function (eq. [C4]) and substitute $\hat{h}$ from equation (C6) into the velocity integral. This gives

$$\sum_s \frac{q_s^2 n_{0s}}{T_{0s}}\hat{\phi} = \sum_s 2\pi q_s \int_{-\infty}^{\infty} dv_\parallel \int_0^\infty v_\perp \, dv_\perp J_0\left(\frac{k_\perp v_\perp}{\Omega_s}\right)\hat{h}_s$$

$$= \sum_s \frac{q_s^2 n_{0s}}{T_{0s}}\left[\Gamma_0(\alpha_s)\frac{\omega\hat{A}_\parallel}{k_\parallel c} - \Gamma_0(\alpha_s)\xi_s Z(\xi_s)\left(\hat{\phi} - \frac{\omega\hat{A}_\parallel}{k_\parallel c}\right) - \Gamma_1(\alpha_s)\xi_s Z(\xi_s)\frac{T_{0s}}{q_s}\frac{\delta\hat{B}_\parallel}{B_0}\right], \tag{C11}$$

where, in performing the velocity integrals, we have used the definitions given in § C2.

C4. PARALLEL AMPERE'S LAW

Following a similar sequence of steps for the parallel Ampère's law, equation (A28), we have

$$k_\perp^2\hat{A}_\parallel = \frac{4\pi}{c}\sum_s 2\pi q_s \int_{-\infty}^{\infty} dv_\parallel \int_0^\infty v_\perp \, dv_\perp J_0\left(\frac{k_\perp v_\perp}{\Omega_s}\right)v_\parallel\hat{h}_s$$

$$= -\frac{4\pi\omega}{ck_\parallel}\sum_s \frac{q_s^2 n_{0s}}{T_{0s}}[1 + \xi_s Z(\xi_s)]\left[\Gamma_0(\alpha_s)\left(\hat{\phi} - \frac{\omega\hat{A}_\parallel}{k_\parallel c}\right) + \Gamma_1(\alpha_s)\frac{T_{0s}}{q_s}\frac{\delta\hat{B}_\parallel}{B_0}\right]. \tag{C12}$$

C5. PERPENDICULAR AMPÈRE'S LAW

It is convenient to take the divergence of the perpendicular Ampère's law, equation (A29), before processing it in the same way as the two other field equations. This gives

$$\frac{\delta \hat{B}_\parallel}{B_0} = -\frac{4\pi}{B_0^2} \sum_s 2\pi T_{0s} \int_{-\infty}^{\infty} dv_\parallel \int_0^{\infty} v_\perp \, dv_\perp \frac{2v_\perp^2}{v_{\mathrm{th}_s}^2} \frac{J_1(k_\perp v_\perp/\Omega_s)}{k_\perp v_\perp/\Omega_s} \hat{h}_s$$

$$= -\frac{4\pi}{B_0^2} \sum_s q_s n_{0s} \left[\Gamma_1(\alpha_s) \frac{\omega \hat{A}_\parallel}{k_\parallel c} - \Gamma_1(\alpha_s) \xi_s Z(\xi_s) \left(\hat{\phi} - \frac{\omega \hat{A}_\parallel}{k_\parallel c} \right) - 2\Gamma_1(\alpha_s) \xi_s Z(\xi_s) \frac{T_{0s}}{q_s} \frac{\delta \hat{B}_\parallel}{B_0} \right]. \tag{C13}$$

C6. DISPERSION RELATION

Before combining the three field equations derived above to produce the dispersion relation, we specify a hydrogen plasma, allowing us to take $n_{0i} = n_{0e}$ and $q_i = -q_e = e$. We now divide equation (C11) by $q_i^2 n_{0i}/T_{0i}$, equation (C12) by $(4\pi\omega/ck_\parallel)(q_i^2 n_{0i}/T_{0i})$, and equation (C13) by $(4\pi/B_0^2)q_i n_{0i}$. Noting two manipulations,

$$\frac{k_\perp^2 k_\parallel^2 c^2}{4\pi\omega^2} \frac{T_{0i}}{q_i^2 n_{0i}} = \frac{k_\perp^2 \rho_i^2}{2} \frac{k_\parallel^2 v_A^2}{\omega^2} \quad \text{and} \quad \frac{B_0^2}{4\pi n_{0i} q_i} = \frac{2}{\beta_i} \frac{T_{0i}}{q_i}, \tag{C14}$$

we arrive at an algebraic linear system of equations that can be written succinctly in matrix form as

$$\begin{pmatrix} A & A - B & C \\ A - B & A - B - \dfrac{\alpha_i}{\overline{\omega}^2} & C + E \\ C & C + E & D - \dfrac{2}{\beta_i} \end{pmatrix} \begin{bmatrix} \hat{\phi} \\ -\dfrac{\omega \hat{A}_\parallel}{k_\parallel c} \\ \left(\dfrac{T_{0i}}{q_i}\right) \dfrac{\delta \hat{B}_\parallel}{B_0} \end{bmatrix} = 0, \tag{C15}$$

where $\overline{\omega} = \omega/|k_\parallel|v_A$ and the definitions of the coefficients A, B, C, D, and E are given in equations (42)–(46). Setting the determinant of this matrix equal to zero gives the dispersion relation for linear, collisionless gyrokinetics (eq. [41])

$$\left(\frac{\alpha_i A}{\overline{\omega}^2} - AB + B^2 \right) \left(\frac{2A}{\beta_i} - AD + C^2 \right) = (AE + BC)^2. \tag{C16}$$

The left-hand side of equation (C16) contains two factors, the first corresponding to the Alfvén wave branch and the second to the slow-wave branch; the right-hand side represents a finite Larmor radius coupling between the Alfvén and slow modes that occurs as $k_\perp \rho_i$ approaches unity.

APPENDIX D

ANALYTICAL LIMITS OF THE DISPERSION RELATION

The linear, collisionless dispersion relation equation (41) harbors the plasma dispersion functions $Z(\xi_s)$ and the integrals of the Bessel functions over the perpendicular velocity $\Gamma_0(\alpha_s)$ and $\Gamma_1(\alpha_s)$. These functions can be expanded for large and small arguments, allowing an analytical form of the dispersion relation to be derived in these limits. The arguments in which the expansions are made are

$$\xi_i = \frac{\omega}{|k_\parallel|v_{\mathrm{th}_i}} = \frac{\overline{\omega}}{\sqrt{\beta_i}}, \quad \xi_e = \frac{\omega}{|k_\parallel|v_{\mathrm{th}_e}} = \xi_i \left(\frac{m_e}{m_i} \right)^{1/2} \left(\frac{T_{0i}}{T_{0e}} \right)^{1/2},$$

$$\alpha_i = \frac{(k_\perp \rho_i)^2}{2}, \quad \alpha_e = \frac{(k_\perp \rho_e)^2}{2} = \alpha_i \frac{m_e}{m_i} \frac{T_{0e}}{T_{0i}}. \tag{D1}$$

Thus, the natural subsidiary expansion parameters in the dispersion relation are α_i, β_i, m_e/m_i, and T_{0i}/T_{0e}. The long perpendicular wavelength limit, $\alpha_i \ll 1$, discussed in § 2.6.1, illuminates the physical meaning of each of the factors in the dispersion relation through a connection to the MHD Alfvén and slow modes. In the short-wavelength limit, $\alpha_i \gg 1$, discussed in § 2.6.2, kinetic Alfvén waves replace the MHD modes. In this appendix, we examine the limits of high and low β_i, while keeping α_i finite. This allows us to connect the large- and small-wavelength asymptotics.

D1. HIGH-β LIMIT, $\beta_i \gg 1$

For $\beta_i \gg 1$, we use the small-argument expansion of the plasma dispersion functions, $Z(\xi_s) \simeq i\sqrt{\pi}$, because $\xi_i = \overline{\omega}/\beta_i^{1/2} \ll 1$ and $\xi_e = (m_e/m_i)^{1/2}(T_{0i}/T_{0e})^{1/2}\xi_i \ll 1$. To ensure the latter to be true, we need $T_{0i}/T_{0e} \ll (m_i/m_e)\beta_i$, which is not at all very restrictive. We can also take $\alpha_e \ll 1$ because $m_e/m_i \ll 1$. The coefficients of the gyrokinetic dispersion relation become

$$A \simeq 1 + \frac{T_{0i}}{T_{0e}} + i\sqrt{\pi}\xi_i \left[\Gamma_0(\alpha_i) + \left(\frac{T_{0i}}{T_{0e}}\right)^{3/2}\left(\frac{m_e}{m_i}\right)^{1/2} \right], \tag{D2}$$

$$B \simeq 1 - \Gamma_0(\alpha_i), \tag{D3}$$

$$C \simeq i\sqrt{\pi}\xi_i \left[\Gamma_1(\alpha_i) - \left(\frac{T_{0i}}{T_{0e}}\frac{m_e}{m_i}\right)^{1/2} \right], \tag{D4}$$

$$D \simeq 2i\sqrt{\pi}\xi_i \left[\Gamma_1(\alpha_i) + \left(\frac{T_{0e}}{T_{0i}}\frac{m_e}{m_i}\right)^{1/2} \right] \equiv 2i\sqrt{\pi}\xi_i G(\alpha_i), \tag{D5}$$

$$E \simeq \Gamma_1(\alpha_i) - 1, \tag{D6}$$

where we have dropped all terms of order 1 and higher in m_e/m_i. The auxiliary function $G(\alpha_i)$ introduced in the expression for D is useful below. We see that there are two interesting limits: $k_\perp \rho_i \sim O(\beta_i^{-1/4})$, $\overline{\omega} \sim O(1)$ and $k_\perp \rho_i \sim O(1)$, $\overline{\omega} \sim O(\beta_i^{-1/2})$ (the ordering of $\overline{\omega}$ is assumed a priori and verified by the result, in the usual fashion).

D1.1. The Limit $k_\perp \rho_i \sim 1/\beta_i^{1/4}$

In this ordering, $\alpha_i \sim \xi_i \sim O(\beta_i^{-1/2})$. Expanding $\Gamma_0(\alpha_i) \sim 1 - \alpha_i$ and $\Gamma_1(\alpha_i) \sim 1 - (3/2)\alpha_i$, we find that $A \sim O(1)$ and B, C, D, and $E \sim O(\beta_i^{-1/2})$. The dispersion relation becomes

$$-\left(\frac{\alpha_i}{\overline{\omega}^2} - B\right)D = E^2, \tag{D7}$$

where $B \simeq \alpha_i$, $E \simeq -(3/2)\alpha_i$, and $D \simeq 2i\overline{\omega}(\pi/\beta_i)^{1/2}$. This is a quadratic equation for $\overline{\omega}$. Its solution is

$$\overline{\omega} = -i\frac{9}{16}\sqrt{\frac{\beta_i}{\pi}}\alpha_i \pm \sqrt{1 - \left(\frac{9}{16}\sqrt{\frac{\beta_i}{\pi}}\alpha_i\right)^2}, \tag{D8}$$

which agrees with the a priori ordering $\overline{\omega} \sim O(1)$.

In the limit $k_\perp \rho_i \ll \beta_i^{-1/4}$, we recover, as expected, the Alfvén wave with weak damping (see eqs. [52] and [53]):

$$\overline{\omega} = \pm 1 - i\frac{9}{16}\frac{k_\perp^2 \rho_i^2}{2}\sqrt{\frac{\beta_i}{\pi}}. \tag{D9}$$

For $\alpha_i > (16/9)\sqrt{\pi/\beta_i}$, the frequency is purely imaginary. In the intermediate asymptotic limit $\beta_i^{-1/4} \ll k_\perp \rho_i \ll 1$, we have

$$\overline{\omega} = -i\frac{8}{9}\left(\frac{k_\perp^2 \rho_i^2}{2}\right)^{-1}\sqrt{\frac{\pi}{\beta_i}}, \quad \text{weakly damped,} \tag{D10}$$

$$\overline{\omega} = -i\frac{9}{8}\frac{k_\perp^2 \rho_i^2}{2}\sqrt{\frac{\beta_i}{\pi}}, \quad \text{strongly damped.} \tag{D11}$$

D1.2. The Limit $k_\perp \rho_i \sim 1$

In this ordering, $\alpha_i \sim O(1)$, and $\xi_i \sim O(\beta_i^{-1})$. Then A, B, and $E \sim O(1)$, and C and $D \sim O(\beta_i^{-1})$. The dispersion relation now is

$$\frac{\alpha_i}{\overline{\omega}^2}\left(\frac{2}{\beta_i} - D\right) = E^2. \tag{D12}$$

Since $D \simeq 2i\overline{\omega}(\pi/\beta_i)^{1/2}G(\alpha_i)$, this is again a quadratic equation for $\overline{\omega}$. Its solution is

$$\overline{\omega} = -i\sqrt{\frac{\pi}{\beta_i}}\frac{\alpha_i G(\alpha_i)}{[\Gamma_1(\alpha_i) - 1]^2} \pm \sqrt{\frac{2}{\beta_i}\frac{\alpha_i}{[\Gamma_1(\alpha_i) - 1]^2} - \left\{\sqrt{\frac{\pi}{\beta_i}}\frac{\alpha_i G(\alpha_i)}{[\Gamma_1(\alpha_i) - 1]^2}\right\}^2}, \tag{D13}$$

which agrees with the a priori ordering $\overline{\omega} \sim O(\beta_i^{-1/2})$.
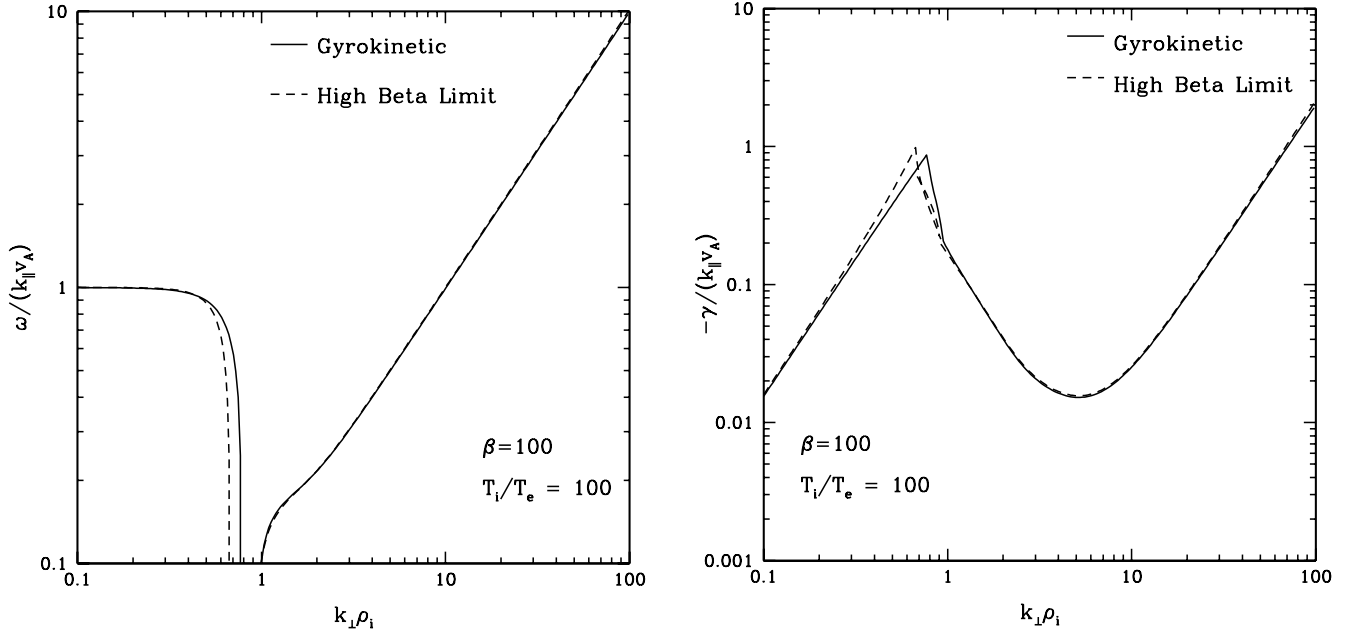
FIG. 9.—Real frequency (*left*) and damping rate (*right*) of the weakly damped Alfvén mode derived by numerical solution of the linear, collisionless gyrokinetic dispersion relation (*solid line*) compared to the high-β analytical limit (*dashed line*). The approximate solution consists of two solutions, valid for $k_\perp \rho_i \sim O(\beta_i^{-1/4})$ and $k_\perp \rho_i \sim O(1)$ (the + branch of eq. [D8] and the − branch of eq. [D13], respectively). In the intermediate limit $\beta_i^{-1/4} \ll k_\perp \rho_i \ll 1$, both solutions are plotted to confirm that they match.

In the limit $k_\perp \rho_i \ll 1$, the two solutions are

$$\overline{\omega} = -\frac{i}{\sqrt{\pi \beta_i}}, \tag{D14}$$

$$\overline{\omega} = -i\frac{8}{9}\left(\frac{k_\perp^2 \rho_i^2}{2}\right)^{-1}\sqrt{\frac{\pi}{\beta_i}}. \tag{D15}$$

The first solution is the damped slow mode (eq. [56]); the second solution matches the weakly damped Alfvén mode in the intermediate limit (eq. [D10]).

In the limit $k_\perp \rho_i \gg 1$, $\Gamma_1(\alpha_i) \to 0$, $G(\alpha_i) \to (T_{0e}/T_{0i})^{1/2}(m_e/m_i)^{1/2}$, and equation (D13) reproduces the $\beta_i \gg 1$ limit of kinetic Alfvén waves (see eqs. [62] and [63]):

$$\overline{\omega} = \pm\frac{k_\perp \rho_i}{\sqrt{\beta_i}} - i\frac{k_\perp^2 \rho_i^2}{2}\sqrt{\frac{\pi}{\beta_i}}\left(\frac{T_{0e}}{T_{0i}}\frac{m_e}{m_i}\right)^{1/2}. \tag{D16}$$

D1.3. Summary

Thus, at $k_\perp \rho_i \sim \beta^{-1/4}$, the low-frequency weakly damped Alfvén waves (eq. [D9]) are converted into two aperiodic modes, one weakly and one strongly damped (eqs. [D10] and [D11]). At $k_\perp \rho_i \sim 1$, the weakly damped Alfvén mode and the weakly damped slow mode (eq. [D14]) are converted into two weakly damped kinetic Alfvén waves (eq. [D16]). These are finally damped at $k_\perp \rho_e \sim 1$. Note that the slow mode we are referring to is the weakest damped of many modes into which the two MHD slow waves and the entropy mode are converted when their parallel wavelengths exceed the ion mean free path. The real frequency and damping rate for $\beta_i = 100$ and $T_{0i}/T_{0e} = 100$ for the branch corresponding to the weakly damped Alfvén mode are plotted in Figure 9.

D2. LOW-β LIMIT, $\beta_i \ll 1$

For $\beta_i \ll 1$, it turns out that A, B, C, D, and $E \sim O(1)$, so the gyrokinetic dispersion relation reduces to

$$\left(\frac{\alpha_i A}{\overline{\omega}^2} - AB + B^2\right)\frac{2A}{\beta_i} = 0. \tag{D17}$$

We focus on the first factor, which corresponds to Alfvén modes (the long-wavelength limit of the second factor gives the ion acoustic wave, see § 2.6.1). We order $\overline{\omega} \sim O(1)$ and consider two interesting limits: $(m_e/m_i)(T_{0i}/T_{0e}) \ll \beta_i \ll 1$ and $\beta_i \sim m_e/m_i \ll 1$, $T_{0i}/T_{0e} \gg 1$. The solutions in these two limits are presented below. These solutions are plotted together with numerical solutions of the full dispersion relation in Figure 10.
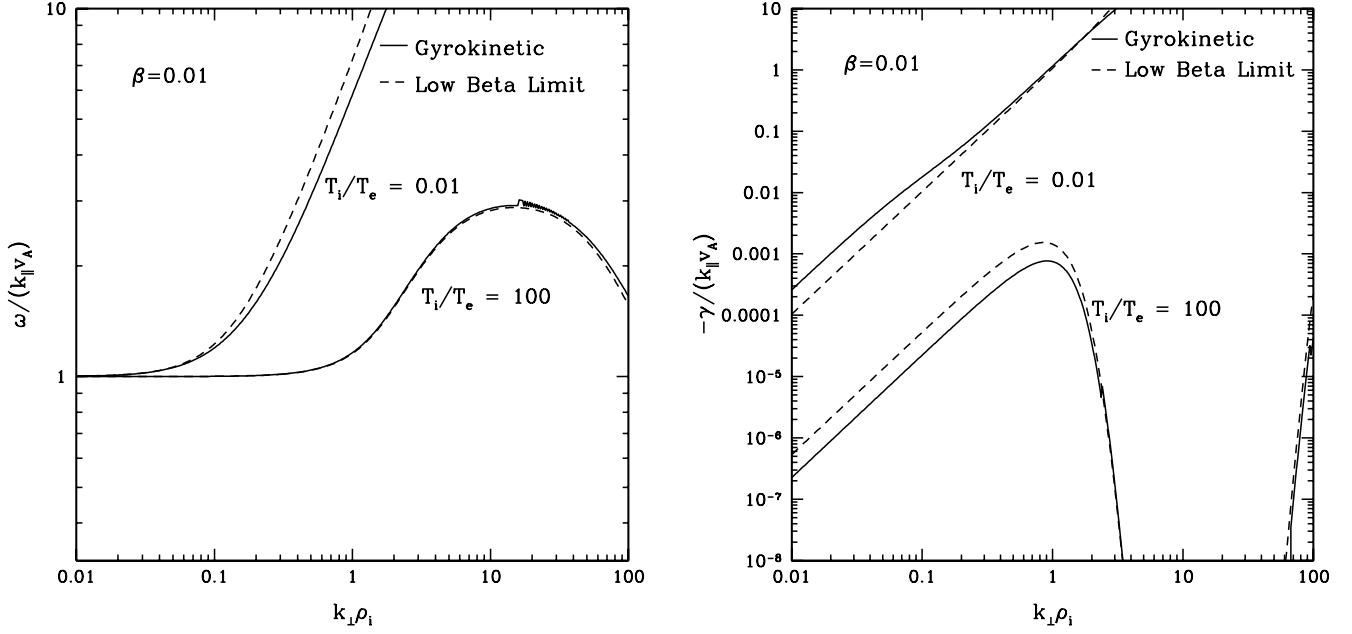
Fig. 10.—Real frequency (*left*) and damping rate (*right*) of the Alfvén mode derived by numerical solution of the linear, collisionless gyrokinetic dispersion relation (*solid line*) compared to the low-β analytical limits $T_{0i}/T_{0e} \gg 1$ (eqs. [D24] and [D25]) and $T_{0i}/T_{0e} \ll (m_i/m_e)\beta_i$ (eqs. [D20] and [D21]).

D2.1. The Limit $(m_e/m_i)(T_{0i}/T_{0e}) \ll \beta_i \ll 1$

In this limit, $\xi_i = \overline{\omega}/\sqrt{\beta_i} \gg 1$ and $\xi_e = (m_e/m_i)^{1/2}(T_{0i}/T_{0e})^{1/2}\xi_i \ll 1$ (slow ions, fast electrons). Expanding the ion and electron plasma dispersion functions in large and small arguments, respectively, we get

$$A \simeq 1 - \Gamma_0(\alpha_i) + \frac{T_{0i}}{T_{0e}} + i\overline{\omega}\sqrt{\frac{\pi}{\beta_i}}\left[\Gamma_0(\alpha_i)\exp\left(-\frac{\overline{\omega}^2}{\beta_i}\right) + \left(\frac{T_{0i}}{T_{0e}}\right)^{3/2}\left(\frac{m_e}{m_i}\right)^{1/2}\Gamma_0(\alpha_e)\right]. \tag{D18}$$

The resulting dispersion relation is

$$\frac{T_{0i}}{T_{0e}}B\Gamma_0(\alpha_e)\overline{\omega}^2 - \alpha_i\left[1 - \Gamma_0(\alpha_i) + \frac{T_{0i}}{T_{0e}}\right] = -i(B\overline{\omega}^2 - \alpha_i)\mathrm{Im}(A), \tag{D19}$$

where the right-hand side is small, so we can solve perturbatively for real frequency and small damping. The result is

$$\overline{\omega} = \pm\sqrt{\frac{\alpha_i[1 - \Gamma_0(\alpha_i) + T_{0i}/T_{0e}]}{(T_{0i}/T_{0e})B\Gamma_0(\alpha_e)}}, \tag{D20}$$

$$\overline{\gamma} = -\frac{\alpha_i}{2[(T_{0i}/T_{0e})\Gamma_0(\alpha_e)]^2}\sqrt{\frac{\pi}{\beta_i}}\left[\Gamma_0(\alpha_i)\exp\left(-\frac{\overline{\omega}^2}{\beta_i}\right) + \left(\frac{T_{0i}}{T_{0e}}\right)^{3/2}\left(\frac{m_e}{m_i}\right)^{1/2}\Gamma_0(\alpha_e)\right], \tag{D21}$$

where $\overline{\gamma} = \mathrm{Im}(\omega)/|k_\parallel|v_A$. Note that $\overline{\omega} \sim O(1)$, as promised at the outset. In the limit α_i and $\alpha_e \ll 1$, equation (D20) reduces to the Alfvén wave solution, $\overline{\omega} = \pm 1$.

D2.2. The Limit $\beta_i \sim m_e/m_i \ll 1, T_{0i}/T_{0e} \gg 1$

In this limit, $\xi_i \sim (m_i/m_e)^{1/2} \gg 1$, and therefore, $\xi_e \sim (T_{0i}/T_{0e})^{1/2} \gg 1$ (both ions and electrons are slow). Expanding all plasma dispersion functions in large arguments, we get

$$A \simeq B - \frac{\Gamma_0(\alpha_e)}{2\overline{\omega}^2}\frac{m_i}{m_e}\beta_i + i\overline{\omega}\sqrt{\frac{\pi}{\beta_i}}\left[\Gamma_0(\alpha_i)\exp\left(-\frac{\overline{\omega}^2}{\beta_i}\right) + \left(\frac{T_{0i}}{T_{0e}}\right)^{3/2}\left(\frac{m_e}{m_i}\right)^{1/2}\Gamma_0(\alpha_e)\exp\left(-\frac{T_{0i}}{T_{0e}}\frac{m_e}{m_i}\frac{\overline{\omega}^2}{\beta_i}\right)\right]. \tag{D22}$$

The resulting dispersion relation is

$$\frac{\alpha_i\Gamma_0(\alpha_e)}{2\overline{\omega}^2}\frac{m_i}{m_e}\beta_i - B\left[\alpha_i + \frac{\Gamma_0(\alpha_e)}{2}\frac{m_i}{m_e}\beta_i\right] = -i(B\overline{\omega}^2 - \alpha_i)\mathrm{Im}(A), \tag{D23}$$

where again the right-hand side is small and solving perturbatively gives

$$\overline{\omega} = \pm \sqrt{\frac{\alpha_i \Gamma_0(\alpha_e)(m_i/m_e)\beta_i}{[2\alpha_i + \Gamma_0(\alpha_e)(m_i/m_e)\beta_i]B}}, \tag{D24}$$

$$\overline{\gamma} = -\frac{2\alpha_i^3 \Gamma_0(\alpha_e)(m_i/m_e)\beta_i}{[2\alpha_i + \Gamma_0(\alpha_e)(m_i/m_e)\beta_i]^3 B^2} \sqrt{\frac{\pi}{\beta_i}} \left[\Gamma_0(\alpha_i) \exp\left(-\frac{\overline{\omega}^2}{\beta_i}\right) \right] + \left[\left(\frac{T_{0i}}{T_{0e}}\right)^{3/2} \left(\frac{m_e}{m_i}\right)^{1/2} \Gamma_0(\alpha_e) \exp\left(-\frac{T_{0i}}{T_{0e}}\frac{m_e}{m_i}\frac{\overline{\omega}^2}{\beta_i}\right) \right]. \tag{D25}$$

REFERENCES

Abramowitz, M., & Stegun, I. A. 1972, Handbook of Mathematical Functions (9th ed.; New York: Dover)
Antonsen, T. M., & Lane, B. 1980, Phys. Fluids, 23, 1205
Armstrong, J. W., Rickett, B. J., & Spangler, S. R. 1995, ApJ, 443, 209
Bale, S. D., Kellogg, P. J., Mozer, F. S., Horbury, T. S., & Reme, H. 2005, Phys. Rev. Lett., 94, 215002
Barnes, A. 1966, Phys. Fluids, 9, 1483
Beer, M. A., Cowley, S. C., & Hammett, G. W. 1995, Phys. Plasmas, 2, 2687
Belcher, J. W., & Davis, L. 1971, J. Geophys. Res., 76, 3534
Brizard, A. 1992, Phys. Fluids B, 4, 1213
Candy, J., Waltz, R. E., & Dorland, W. 2004, Phys. Plasmas, 11, L25
Catto, P. J. 1978, Plasma Phys., 20, 719
Catto, P. J., Tang, W. M., & Baldwin, D. E. 1981, Plasma Phys., 23, 639
Chandran, B. D. G. 2006, Phys. Rev. Lett., in press (astro-ph/0511586).
Cho, J., & Lazarian, A. 2003, MNRAS, 345, 325
Cho, J., Lazarian, A., & Vishniac, E. T. 2002, ApJ, 564, 291
Cranmer, S. R. & van Ballegooijen, A. A. 2003, ApJ, 594, 573
———. 2005, ApJS, 156, 265
Dennett-Thorpe, J., & de Bruyn, A. G. 2003, A&A, 404, 113
Dimits, A. M., Williams, T. J., Byers, J. A., & Cohen, B. I. 1996, Phys. Rev. Lett., 77, 71
Dorland, W., Jenko, F., Kotschenreuther, M., & Rogers, B. N. 2000, Phys. Rev. Lett., 85, 5579
Dubin, D. H. E., Krommes, J. A., Oberman, C., & Lee, W. W. 1983, Phys. Fluids, 26, 3524
Ernst, D. R., et al. 2004, Phys. Plasmas, 11, 2637
Foote, E. A., & Kulsrud, R. M. 1979, ApJ, 233, 302
Fried, B. D., & Conte, S. D. 1961, The Plasma Dispersion Function (New York: Academic Press)
Frieman, E. A., & Chen, L. 1982, Phys. Fluids, 25, 502
Goldreich, P., & Sridhar, S. 1995, ApJ, 438, 763 (GS95)
———. 1997, ApJ, 485, 680
Goldstein, M. L., Roberts, D. A., & Matthaeus, W. H. 1995, ARA&A, 33, 283
Gruzinov, A. 1998, ApJ, 501, 787
Hahm, T. S., Lee, W. W., & Brizard, A. 1988, Phys. Fluids, 31, 1940
Helander, P., & Sigmar, D. J. 2002, Collisional Transport in Magnetized Plasmas (Cambridge: Cambridge Univ. Press)
Jenko, F., & Dorland, W. 2001, Plasma Phys. Control. Fusion, 43, A141
———. 2002, Phys. Rev. Lett., 89, 225001
Jenko, F., Dorland, W., & Hammett, G. W. 2001, Phys. Plasmas, 8, 4096
Jenko, F., Dorland, W., Kotschenreuther, M., & Rogers, B. N. 2000, Phys. Plasmas, 7, 1094
Kingsep, A. S., Chukbar, K. V., & Yankov, V. V. 1990, Rev. Plasma Phys., 16, 24
Kolmogorov, A. N. 1941, Dokl. Akad. Nauk SSSR, 30, 9
Kotschenreuther, M., Rewoldt, G., & Tang, W. M. 1995, Comp. Phys. Comm., 88, 128

Krall, N. A., & Trivelpiece, A. W. 1986, Principles of Plasma Physics (New York: McGraw-Hill)
Krommes, J. A. 1999, Phys. Plasmas, 6, 1477
Krommes, J. A., & Hu, G. 1994, Phys. Plasmas, 1, 3211
Leamon, R. J., Matthaeus, W. H., Smith, C. W., Zank, G. P., Mullan, D. J., & Oughton, S. 2000, ApJ, 537, 1054
Leamon, R. J., Smith, C. W., Ness, N. F., Matthaeus, W. H., & Wong, H. K. 1998, J. Geophys. Res., 103, 4775
Leamon, R. J., Smith, C. W., Ness, N. F., & Wong, H. K. 1999, J. Geophys. Res., 104, 22331
Lee, W. W. 1983, Phys. Fluids, 26, 556
———. 1987, J. Comput. Phys., 72, 243
Lifshitz, E. M., & Pitaevskii, L. P. 1981, Physical Kinetics (Oxford: Pergamon Press)
Lithwick, Y., & Goldreich, P. 2001, ApJ, 562, 279
Maron, J., & Goldreich, P. 2001, ApJ, 554, 1175
Matthaeus, W. H., Goldstein, M. L., & Roberts, D. A. 1990, J. Geophys. Res., 95, 20673
Montgomery, D., & Turner, L. 1981, Phys. Fluids, 24, 825
Parker, S. E., Chen, Y., Wan, W., Cohen, B. I., & Nevins, W. M. 2004, Phys. Plasmas, 11, 2594
Qin, H., Tang, W. M., & Lee, W. W. 2000, Phys. Plasmas, 7, 4433
Quataert, E. 1998, ApJ, 500, 978
Quataert, E., & Gruzinov, A. 1999, ApJ, 520, 248
Rickett, B. J., Kedziora-Chudczer, L., & Jauncey, D. L. 2002, ApJ, 581, 103
Rogers, B. N., Dorland, W., & Kotschenreuther, M. 2000, Phys. Rev. Lett., 85, 5336
Rutherford, P. H., & Frieman, E. A. 1968, Phys. Fluids, 11, 569
Schekochihin, A. A., & Cowley, S. C. 2006a, in Magnetohydrodynamics: Historical Evolution and Trends, ed. S. Molokov, R. Moreau, & H. K. Moffatt (Berlin: Springer), in press (astro-ph/0507686)
———. 2006b, Phys. Plasmas, 13, 056501
Schekochihin, A. A., Cowley, S. C., Dorland, W. D., Hammett, G. W., Howes, G. G., & Quataert, E. 2006, ApJ, in press
Shebalin, J. V., Matthaeus, W. H., & Montgomery, D. 1983, J. Plasma Phys., 29, 525
Spangler, S. R., & Gwinn, C. R. 1990, ApJ, 353, L29
Sridhar, S., & Goldreich, P. 1994, ApJ, 432, 612
Stix, T. H. 1992, Waves in Plasmas (New York: AIP)
Taylor, J. B., & Hastie, R. J. 1968, Phys. Fluids, 10, 479
Trotter, A. S., Moran, J. M., & Rodríguez, L. F. 1998, ApJ, 493, 666
Watson, G. N. 1966, A Treatise on the Theory of Bessel Functions (2nd ed.; Cambridge: Cambridge Univ. Press)
Wilkinson, P. N., Narayan, R., & Spencer, R. E. 1994, MNRAS, 269, 67